UNIVERSITÀ DEGLI STUDI DI PADOVA

DIPARTIMENTO DI BIOLOGIA

Corso di Laurea magistrale in *Molecular Biology*

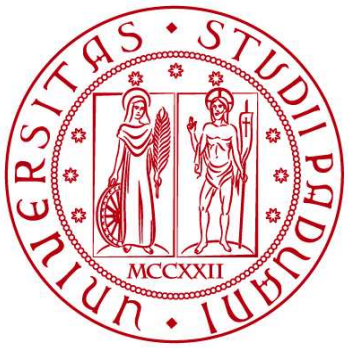

TESI DI LAUREA

Physiological characterization of *Physcomitrium patens* lines with different levels of expression of flavodiiron proteins

Relatore**: Prof.** ***Tomas Morosinotto***
Dipartimento di Biologia

Laureando**:** ***Emma Zampieri***

ANNO ACCADEMICO 2022/2023

A Giulia, e a tutte le donne
che ogni giorno lottano
per cambiare il mondo

Summary

Abstract

Photosynthetic organisms are constantly exposed to light stress and, to avoid photodamage, they evolved several strategies to sidestep electrons accumulation. Indeed, electrons excited at photosystem II (PSII) and photosystem I (PSI) level can follow the linear electron flow (LEF) to the Calvin-Benson cycle (CBC) or the alternative electron pathways. Cyclic electron transports (CET) and pseudo-cyclic electron transports (PCET) constitute the most conserved ones. While CETs recycle electrons from PSI back to the plastoquinone pool, PCETs use electrons to reduce molecular oxygen into water. FLVs proteins represent the major electron sink among the PCETs resulting indispensable in the dark-to-light transition and under fluctuating light exposure. Homologous sequences of FLVs have been highly conserved during evolution, but they have been lost in angiosperm. *Physcomitrium patens* is a bryophyte widespread used as a model organism and different alternative electron flow co-exist in it, including the heterodimer FlvA/FlvB. In this study, *P. patens* double knock-out mutans have been transformed with WT FLVA and FLVB genes. Molecular and physiological analysis allowed to analyze the effect of the overexpression of one or both flavodiiron proteins, with a focus on the impact on the efficiency of the two photosystems and on the level of photodamage.

1. Introduction

1.1 Oxygenic photosynthesis

From cyanobacteria to green algae and vascular plants, the oxygenic photosynthesis represents the principal way to generate oxygen and organic matter on earth. It is achieved by a series of phototropic reaction that occur mainly in the chloroplast. (Nelson e Ben-Shem 2004). The chloroplast is an organelle characterized by a double membrane envelope: an outer membrane, which is more permeable, and an inner membrane, which controls the ion concentration. Inside the chloroplast a high folded internal membrane system named thylakoid is present. The latter consists in two different morphological structured called grana and stroma lamellae. While the first is a pile of membrane disks, in which the thylakoid lumen allows the formation of a proton motive force to drive the ATP formation, the seconds are external parts of membrane and are appointed to connect the grana stacks (**Figure 1.1a**) (Gao et al. 2018).

Photosystem is based on the phototrophy mechanism by which the energy carried by photons is converted into electrochemical energy. These reactions take place in the so-called reaction centers. The latter, called photosystem in Cyanobacteria, are multisubunit membrane proteins responsible for the transition from light energy to chemical energy. When a photon of light is absorbed by a reaction center, a charge separation event takes place, generating a lower-redox-potential electron donor and a higher-redox-potential electron acceptor (P^+) in two distinct parts of the protein. While the lower-potential electron will be used to do energy conservation or carbon fixation, the hole at P+ is filled by an electron coming from the so called water-water cycle, returning the reaction center to the ground state (**Figure 1.1c**) (Fischer, Hemp, e Johnson 2016).

In all the organisms that perform oxygenic photosynthesis, two types of photosystems are present on the thylakoid membranes: a photosystem I (PSI), placed on the stroma lamellae, and a photosystem II (PSII), found on the grana stacks (**Figure 1.1b**). Both PSI and PSII comprise a core complex and a peripheral antenna system (LHC), LHCI for the PSI and LHCII for the PSII. This last is a structure constituted by light sensitive molecules, such as carotenoids and chlorophylls, able to harvest light and to funnel it to the photosynthetic reaction

centers (RC). In these last, the excitation a chlorophyll molecule able to initiate the proton translocation into the lumen takes place. In particular, the chlorophyll P680 is found in PSII while the chlorophyll P700 belongs to the PSI (Gao et al. 2018).

Oxygenic photosynthesis is complex. The two photosystems are assembled in series, to allow to electron transfer from a water molecule to the ferredoxin and the generation of a proton driven force to generate ATP (Fischer, Hemp, e Johnson 2016). When light reach the chlorophyll P680, a charge separation event take place. The electron transfer led to the oxidation of the P680 with a consequent reduction of the primary electron acceptors, pheophytin (Ph) and plastoquinol (Q_A), sequentially (Gao et al. 2018). At the same time, an electron coming from the redox-active tyrosine, able to harvest electrons from water, fills the electron hole of the $P680^+$. To obtain a fully reduced plastoquinol (Q_B), a second photocycle is required. The Q_B is then moved to the cytochrome b_6f (also indicated as Complex III) that oxidize the plastoquinol and reduce the plastocyanin (PC). The Cyt b_6f allow to maximize the energy conservation, generating a proton mortice force, exploiting the so-called Q cycle ($2H^+$ per electron transferred) (Nelson e Ben-Shem 2004). Since the chlorophyll P700 in the PSI perform a charge separation similar to the one observed in the PSII, leading to an electron hole ($P700^+$), the PC role is to re-reduce it. The electron transfer continues with the reduction of an iron-sulfur cluster, which in turn reduces the ferredoxin. This last, finally, exploit the electron transfer to reduce $NADP^+$ to NADPH, then used in the carbon fixation reactions (**Figure 1.1d**) (Fischer, Hemp, e Johnson 2016).

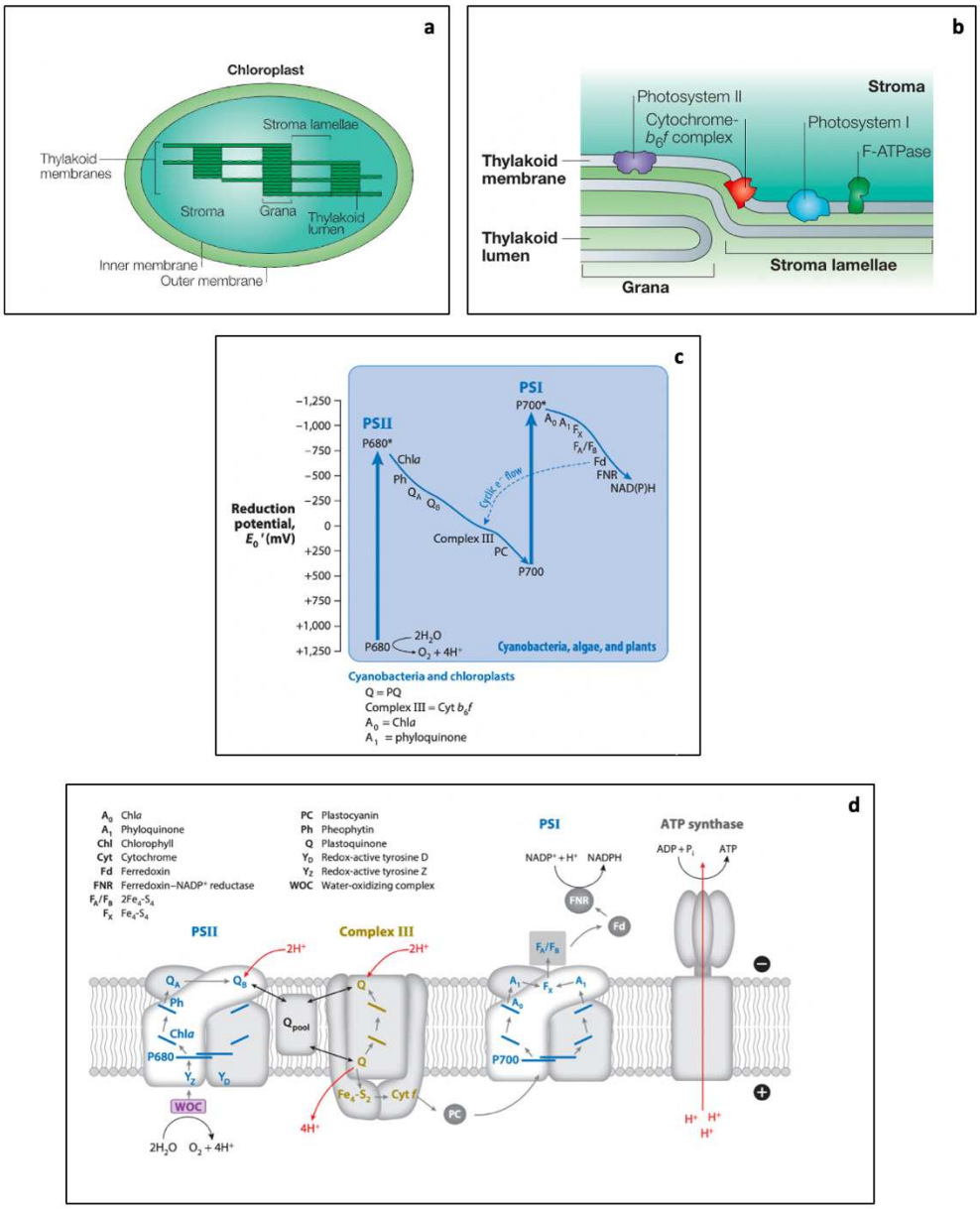

Figure 1.1: ***a.*** *Cross section of the chloroplast organelle in which it is possible to appreciate the double membrane envelope and the thylakoid membrane system inside. In the latter, grana stacks can be distinguished from the thylakoid lamellae (Nelson e Ben-Shem 2004).* ***b.*** *Schematic representation of the multisubunit membrane complexes, such as the PSII, the PSI, the cytochrome b6f and the F-ATPase (Nelson e Ben-Shem 2004).* ***c.*** *Energetics of oxygenic phototrophy. The z scheme shows the electron pathway from the water to the NADP⁺. Arrows illustrate the photoexcitation of electrons by the different reaction centers, and the lengths of the arrows reflect the energies of the excitons (Fischer, Hemp, e Johnson 2016).* ***d.*** *Thylakoid membrane cross section. Electron transport and energy conservation of oxygenic photosynthesis are shown. While grey harrows show the electron flow, the red ones represent the proton translocation. Starting from the water-oxidizing complex, electrons move from the PSII to the Q_{pool}. From there, they flow into complex III (in Cyanobacteria this is cytochrome b6f) and participate in the Q cycle. Then, via plastocyanin (PC), they are supplied to the PSI, where they arrive at ferredoxin. Ferredoxin–NADP+ reductase places them subsequently onto NADPH, which can then be used for carbon fixation, biosynthesis, and aerobic respiration (Fischer, Hemp, e Johnson 2016).*

1.2 Calvin Benson Cycle

In the oxygenic photosynthesis, the Calvin Benson-Bassham (CBB) cycle represent the key step during which, the NADPH and the ATP produced during photochemistry are exploited to fix the CO_2 and to produce organic matter. It is characterized by distinct phases and many different enzymes are involved in the reactions. Since the 60s, it was known that these enzymes are regulated by light. In fact, their activity result dependent by the it: it is low in the dark, while it increases under illumination. This regulation happens thanks to the presence of a regulatory disulfide into the light-depended enzymes, that is oxidize in the dark and reduced in the light. The thioredoxins regulation, as it is called, permit the reduction and thus the passage from a low active enzyme to an full active one (Michelet et al. 2013).
The core carboxylation enzyme of this pathway is ribulose 1,5-bisphosphate carboxylase oxygenase (RUBISCO), whose activity depends on two substrates with different origin: CO_2 from the atmosphere, and ribulose-1,5-bisphosphate (RuBP) that is synthesized from 3-phosphoglycerate (PGA) (Gurrieri et al. 2023). In C3 plants, RUBISCO has not just a carboxylase activity, but it is also able to react with O_2. When this happen, a molecule of PGA and one molecule of 2-phosphoglycolate are produced. To convert the 2-phosphoglycolate back into PGA, the photorespiration cycle is required. It takes place into three different organelles and require both ATP and NADPH (Peterhansel et al. 2010).
As mentioned before, the CCB cycle consists in three different phases: the carboxylation phase, the reduction phase, and the regeneration phase. During the first phase, the ribulose 1,5-bisphosphate (RuBP) is carboxylate by RUBISCO and two molecules of 3-phosphoglycerate (PGA) are produced. The second phase sees the conversion of the PGA into glyceraldehyde-3-phosphate, catalyzed firstly by the phosphoglycerate kinase (PGK) and then by the glyceraldehyde-3-phosphate dehydrogenase (GAPDH), and required both ATP and NADPH. Finally, the last phase is deputed to the regeneration of the RuBP. Different enzymes are involved into it (**Figure 1.2**) (Gurrieri et al. 2023).

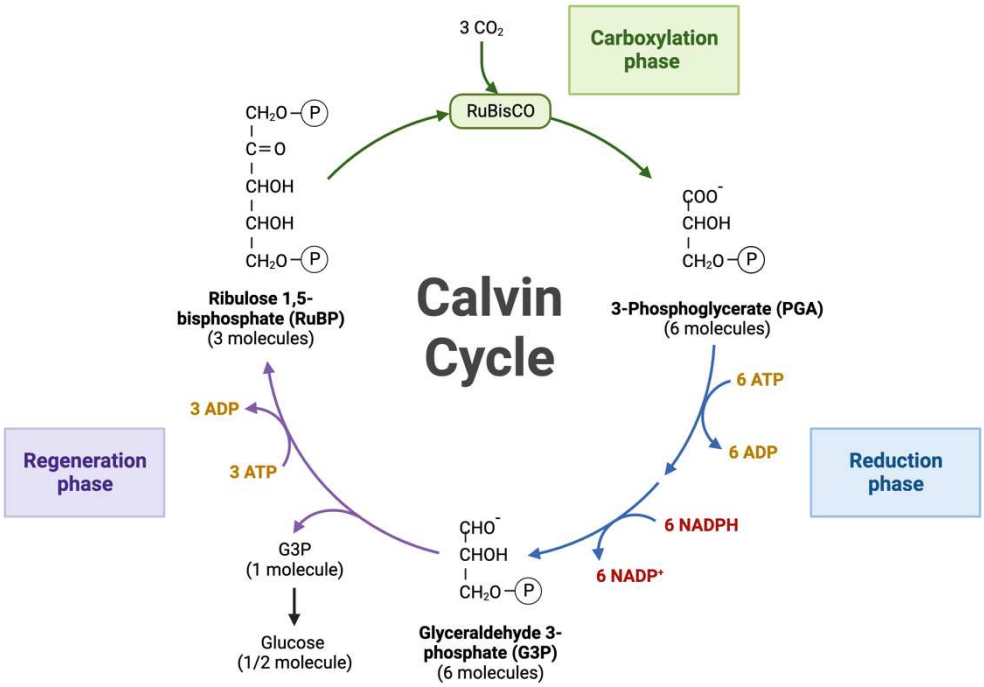

***Figure 1.2**: The Calvin cycle is characterized by three phases, the carboxylation phase, the reduction phase, and the regeneration phases, and they are respectively described by the next three stages. In the stage 1, the enzyme RuBisCO incorporates carbon dioxide into an organic molecule. In stage 2, the organic molecule is reduced. In stage 3, RuBP, the molecule that act at substrate to initiate the cycle, is regenerated (Adapted from "Calvin cycle", by BioRender.com (2023). Retrieved from https://app.biorender.com/biorender-templates).*

1.3 Photosynthetic alternative electron transports

Thanks to the linear electron flow (LEF) that occurs between the PSI and the PSII, a proton motive force (to generate ATP) and NADPH molecules are produced. The carbon fixation is strictly influenced by both ATP and the NADPH level. For this reason, the plant metabolism must be capable to adapt to dynamic environmental conditions, such as the stressful light conditions or the CO_2 and nutrients availability (Alboresi, Storti, e Morosinotto 2019).
Even if the PSII is protect by specialized repair machinery, such as the high turnover of the D2 protein or the dissipation of energy as heat (NPQ), no analogous systems have been discovered in PSI. The latter, under stressful conditions, is subjected to photodamage, with a consequent decrease of its efficiency and thus of the NADPH and ATP production (Alboresi, Storti, e Morosinotto 2019).

The discovery of the alternative electron flow, allowed to better understand how the PSI reacts to the dynamic natural environmental conditions. In particular, these alternative electron pathways are able to regulate the level between the rate of metabolism of ATP/NADPH utilization and the level of energy available, where an unbalance can lead to the production of reactive oxygen species (ROS), that can potentially damage the two photosystems. The goal of the alternative electron flow is thus to diverge the electrons from/to the LEF (**Figure 3.1a**) to modulate the ATP/NADPH ration in an environmental dependent manner (Storti et al. 2019).
The cyclic electron flow (CEF) and the pseudo-cyclic electron flow (PCEF) represent the principal alternative electron pathways to avoid P700 overreduction (**Figure 1.3c**). Their activities are found in all photosynthetic organisms, but they are not equally distributed (**Figure 1.3b**). They have been shown to play a fundamental role in PSI photoprotection and corresponding mutants display PSI damage and sharp growth defects (Alboresi, Storti, e Morosinotto 2019).

1.3.1 CYCLIC ELECTRON FLOW (CEF)

In contrast to what it has been observed in the linear electron transfer, CEF act just around the PSI modulating the NADPH/ATP ratio. In detail, it is able to create a ΔpH and to avoid the NADPH accumulation, promoting proton pumping by cytochrome (Cyt) b_6f (Rochaix 2011). From chlorophyte to angiosperm, the CEF is characterize by two different pathways actuated by the ferredoxin-dependent PQ reduction (**Figure 1.3c**). The first is related to the PGR5/PGRL1 complex and it is sensible to antimycin A. Thanks to experimental analysis in *Arabidopsis pgr5* mutant, it has been demonstrated that the formation of a ΔpH in CEF regulate both the electron transport and the dissipation of energy as heat (NPQ) under high light conditions (Yamamoto et al. 2016). Beside the PGR5/PGRL1 complex CEF, the NADH dehydrogenase-like (NDH) complex has been described. It is a chloroplast multimeric complex and it is not equally distributed in all photosynthetic organisms. Gymnosperm, for example, had lost the NDH gene, while in chlorophyte, the NDH-1 gene has been substituted by the NDH-2 gene, which in turn do not participate to the ΔpH formation (Alboresi, Storti, e Morosinotto 2019).

1.3.2 PSEUDO CYCLIC ELECTRON FLOW

Similarly, to what has been identified CEF, also in PCEF two pathways have been described: the so-called Mehler reaction and the flavodiiron proteins enzyme (FLVs) (**Figure 1.3c**). In the first case, two enzymes (the superoxide dismutase and the ascorbate peroxidase respectively) allow the conversion of the superoxide ion (O_2^-) to H_2O_2, which is successively transform to O_2.
Latterly respect to Mehler reaction discovery, FLVs have been identified. They represent the second PCEF pathway and are able to avoid the over-reduction of the PSI, accepting electrons downstream the photosystem and reducing oxygen into water. While the Mehler reaction are inherited from cyanobacteria to angiosperm, FLVs proteins are unequally distributed. It has been demonstrated that *flv* mutans in *P. patens* show high level of acceptor side limitation when the light intensity, confirming their ability to protect the PSI from photodamage (Alboresi, Storti, e Morosinotto 2019).

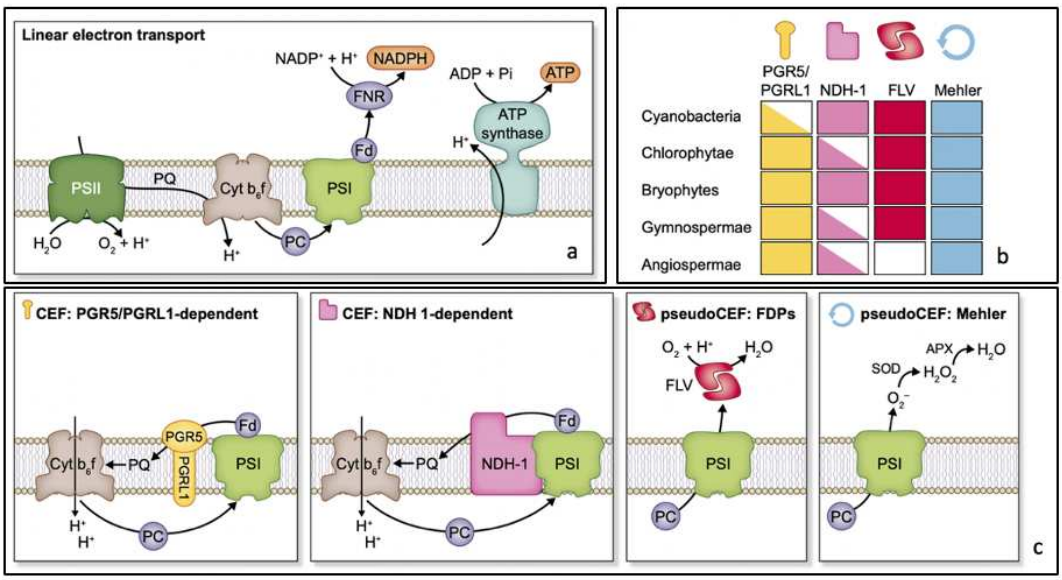

Figure 1.3 (Alboresi, Storti, e Morosinotto 2019): *Diversity and distribution of electron transport pathways in oxygenic photosynthetic organisms.* ***a.*** *Linear electron flow (LEF) implies the transport of electrons from water to NADP+ and the generation of a proton gradient to produce ATP. It occurs on the thylakoid membrane and where the catalysing complexes have been conserved from cyanobacteria to vascular plants.* ***b.*** *Alternative pathways not equally distributed in different phylogenetic groups. their distribution is represented with colour coding to indicate their presence.* ***c.*** *Alternative electron pathways to modulate electron transport efficiency. This modulation involves cyclic electron flow (CEF) around PSI (PGR5/PGRL1-dependent and NDH-1-dependent) and pseudo-CEF (or water–water cycle).*

1.4 Flavodiiron proteins

1.4.1 STRUCTURE AND CLASSIFICATION

Flavodiiron proteins are part of a bigger group of protein, indicated as FDPs, which has been identified in all three domains system: Bacteria, Archaea and Eukarya. Their substrate can be both the nitric oxide (NO) or the oxygen molecule, which are submit to a reduction reaction in order to produce innocuous molecules, such as N_2O or H_2O. In fact, previous experiments demonstrate how the over production of NO can react with oxygen, causing the production of reactive nitrogen species (RNS), that can damage various cell components under anaerobic conditions (Folgosa, Martins, e Teixeira 2018).
The common structure of all FDPs is characterized by the presence of two domains (**Figure 1.4.1a**). At the N-term a metallo β lactamase (MBL) domain is identified (~250 aminoacids). It harbors a di-iron center, which represent the catalytic site to reduce NO or O_2. On the other side, at the C-terminal, a NADPH flavin mononucleotide (FMN) domain is present (~150 aminoacids). Based on the specificity of the C-term domains, the superfamily of FDPs is subdivided into eight different groups, from *class A* to *class H*. Among these, some FDP group are able to reduce preferentially or the NO or the O_2; others act instead on both (Alboresi et al. 2019).
Flavodiiron proteins belong to the *Class-C* FDPs, in which the C-terminal is characterized by the presence of a NADPH dependent flavin oxidoreductase-like domain. They are normally found in photosynthetic organisms and they have been isolated for the first time in the cyanobacterium Synechocystis sp. strain PCC 6803. In the latter, four different FLVs genes have been detected based on the sequence homology: FLV4/FLV4 and FLV1/FLV3. While these last are present only in prokaryotes organisms and show the O_2 reduction both *in vivo* and *in vitro*, FLVA and FLVB represent the homologous sequences of FLV1/FLV3 and they are found in eukaryotic organisms from chlorophyte to gymnosperm. It is interesting to see that FLVs proteins have been lost during evolution. Analysis conducted on angiosperms reveal that these proteins are not present in this photosynthetic group, probably due to a gene loss (Alboresi et al. 2019).
In **Figure 1.4.1b**, a phylogenetic tree is reported. It shows the relative distribution of both FLV1/FLVA and FLV3/FLVB in different photosynthetic organisms. It is immediately clear the phylogenetic separation between the FLVs in prokaryotes (FLV1/FLV3) and in eukaryotes (FLVA/FLVB), as it is evident that

FLVA and FLVB in chlorophyte differentiates from those in streptophytes. As it can be notice, FLV genes are found in couple. This characteristic reflects their inability to work as a single protein. In fact, it has been demonstrated that, if FLV1 or FLV3 gene is expressed in a flv1/flv3 double know-out, the expression of just one of the two proteins is not sufficient to protect PSI from photodamage. Thus, FLVs work as a heterodimer to reduce O_2 into H_2O, downstream the PSI (Alboresi et al. 2019).

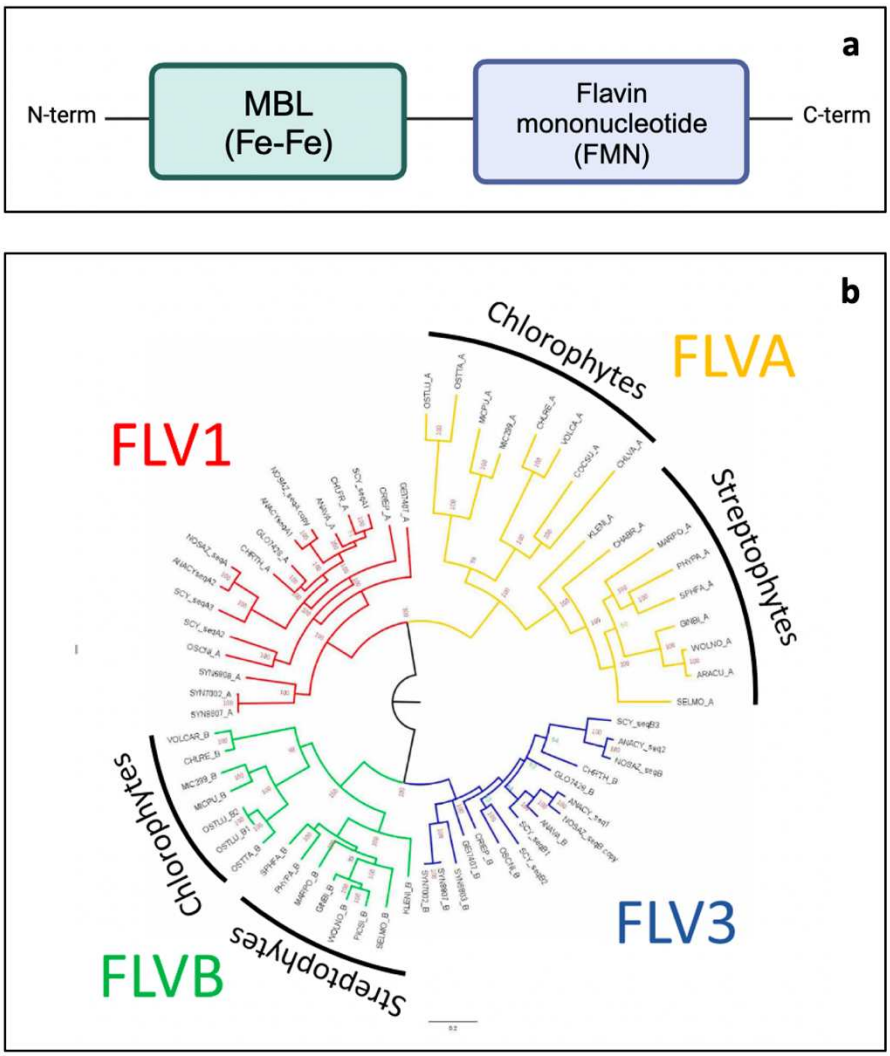

***Figure 1.4.1**: **a.** Schematic representation of the two domains in common between all the eight subgroups of FDPs. At the N-terminal a metallo beta lactamase domain is present, while the C-terminal is characterized by a flavin mononucleotide domain. The C-terminal represent the variable portion of the FDPs proteins along the different subgroups (Alboresi et al. 2019). **b.** Phylogenetic unrooted tree that shows the relative distribution of FLV1/FLV3 and FLVA/FLVB genes. While the first are present in prokaryotes, the second are expressed in eukaryotes. A clear differentiation is detectable also between chlorophyte and streptophytes (Alboresi et al. 2019).*

1.4.2 FUNCTION OF FLVs IN PHOTOSYNTESIS

As described in the previous paragraph, the *class c* FDPs proteins is responsible of the oxidation of the NADPH and of the reduction of O_2 into water. They represent one of the two PCEF pathways identified and are fundamental to protect the two photosystems from photodamage and growth defects.
At the molecular level, the FLVs activity is immediate and lasts a few seconds after the light is switched on, then their action become non-detachable. At the same time both LEF e PCEF activate, but their rate of activation is slower compared to the one in FLVs (**Figure 1.4.2a**) (Alboresi, Storti, e Morosinotto 2019).
FLVs proteins acts downstream the PSI and the depletion of the FLVs sequence is correlated with high level of acceptor side limitation every time that the light intensity increases (**Figure 1.4.2b.c**). In particular, under fluctuating light conditions, when the LEF is limited and the $NADP^+$ availability is low, the FLVs are able to maintain the PSI oxidized (high level of donor side limitation) maintaining univariable the rate of electron transport activity and sustaining the formation of a ΔpH. Moreover, it has been observed that *flv* mutants delay the activation of NPQ due to the over reduction of the PQ pool that reduce the rate of acidification of the thylakoid lumen (Alboresi et al. 2019).
Even if FLVs proteins have been lost during evolution, an experiment performed in (Yamamoto et al. 2016), transformed Arabidopsis and rice with FLVs genes, demonstrating that these proteins do not necessitate accessory elements to be functionally active. On reliable reason can be due to the energy loss in PCEF, during which the electrons are used to produce water and are not re-entered into the LEF of the CEF. This last, in fact, results more efficient in term of electron transport rate (Alboresi, Storti, e Morosinotto 2019).

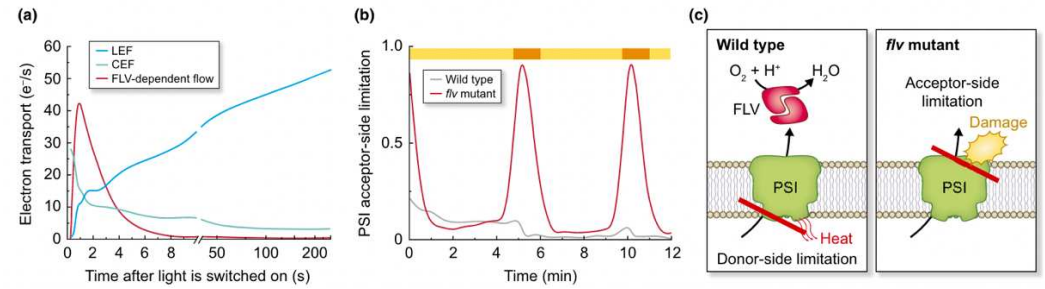

***Figure 1.4.2 (Alboresi, Storti, e Morosinotto 2019)**: FLVs act downstream the PSI, protecting it from photodamage. **a.** Electron transport rate immediately after the light is switched on. Each line represents the relative contribution of different electron transports: LEF (blue), CEF (green) and PCEF related to FLVs (red). **b.** Acceptor side limitation (Y(NA)) levels during a fluctuating light experiment. It is possible to appreciate the increase on the Y(NA) every time the light intensity increases in the flv mutant compared to the WT. **c.** Schematic representation of FLV activity. While the WT present high level of donor side limitation and is able to dissipate the energy as heat, the flv mutant is characterized by a high acceptor side limitation. The last case leads to the electron accumulation, causing the overexcitation of the PSI.*

1.5 Physcomitrium patens as model organism

Among land plants, mosses (Bryophytaea) represent one of the oldest groups. Originated 500 million years ago, they diffuse many different habitats, reaching also the most extreme part of our planet. There are at least 10,000 different species and their evolutionary position is perfect to study the plethora of physiological reactions that occur in land plants (Schaefer e Zrÿd 2001).
Since the 1960s, Physcomitrium patens was primarily used as a genetic system to isolate and analyze mutans in a different process and its genome has been the first sequenced in the non-seed plant group. It represents one of the best suitable model organisms for genetic engineering techniques and it has been observe that transgene are successfully integrated into its genome through homologous recombination (Rensing et al. 2020). Moreover, as part of bryophyte group, P. patens present all the different alternative electron pathways identified until now (Alboresi, Storti, e Morosinotto 2019).

1.5.1 P. Patens LIFE CYCLE

Such as the terrestrial plants, mosses life cycle is haplodiplontic. It is characterized by both a dominant haploid generation and a diploid generation, represented by the gametophyte and the sporophyte respectively. At the level

of the sporophyte, just one capsule is generated, classifying it into the group of the monosporangiate (Rensing et al. 2020).

The life cycle of *P. patens* starts with the germination of the spore. The protonema develops and two type of cells can be identified: the chloronema and caulonema. Together, the latter give origin to a filament structure determinate by the division of the apical and sub apical cells. While chloronema cells are rich of chloroplast, caulonema cells carry less chloroplasts but their rate of division is higher compared to the first. A structure named bud allow the development of a three-dimension stage that allow to produce leaves and the generation of the gametophores. As all the mosses, P. patens is bisexual. During those days in which the light duration in short, male and female reproductive structures originate on the apical part of the gametophore. The female organ is called archegonium while the male organ is called antheridium. In presence of water, thanks to the presence of a flagella, spermatozoid can arrive at the bottom of the archegonium and fertilize the egg. The diploid zygote can originate an embryo and later can allow the generation of spores (2n) (Rensing et al. 2020).

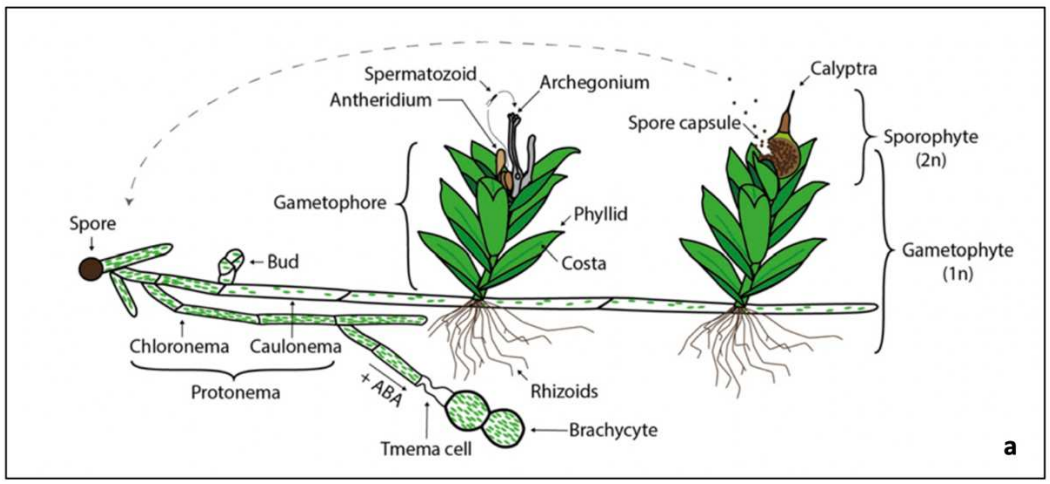

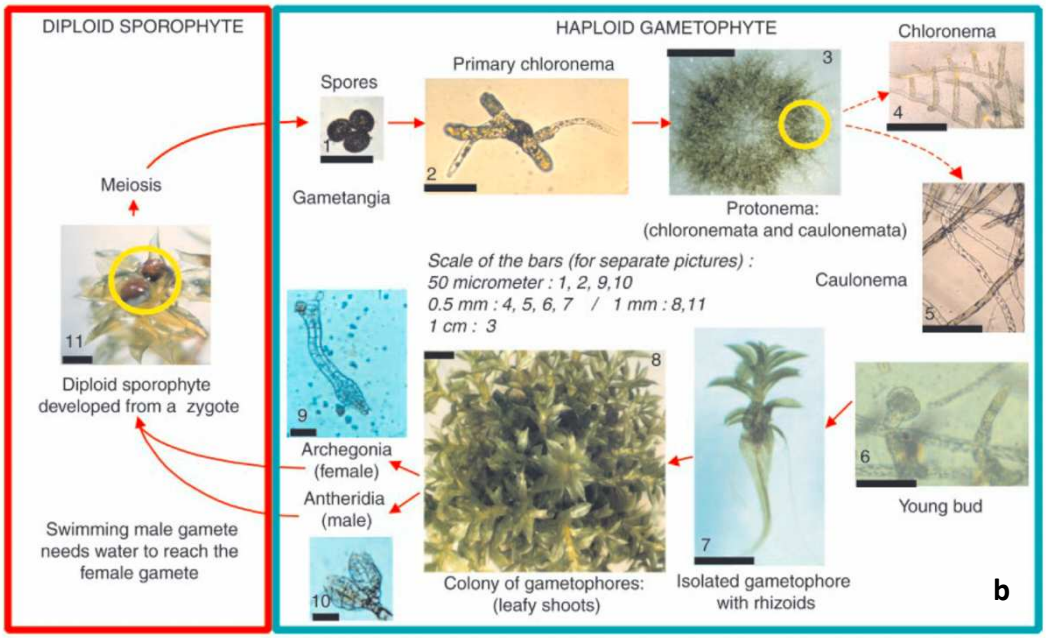

***Figure 1.5.1**: **a.** Life Cycle of and relative structure of P. patens at the microscopy (Rensing et al. 2020). **b.** Life cycle in P. patens in detail. (**1**) Spores. (**2**) Primary chloronema. (**3**) Protonema. (**4-5**) Chloronema and caulonema. (**6**) Bud. (**7**) Gametophore with relative rhizoid. (**8**) Colony of gametophores. (**9**) The two reproductive organs: the archegonia (female) and the antheridia (male) (Schaefer e Zrÿd 2001).*

Thesis aim

The aim of this project is to screen and characterize different lines of *Physcomitrium patens flva/flvb* KO transformed with FLVA and FLVB genes. In particular, two distinct group of strain have been used: the overexpressing *FlvA-FlvB* lines (oeFlvA-FlvB), in which the two genes are expressed independently under the control of a strong promoter (P_{35S}), and the FABOE lines (oeFlvA-2A-FlvB), where the FLVA and FLVB genes are co-expressed (under the control of the same P_{35} strong promoter) and the presence of the 2A peptide guaranteed an independent translation.
Three main goals have been achieved. Firstly, analyze the impact of the over-expression of the flavodiiron proteins under high light and fluctuating light conditions, through the analysis of physiological parameters, such as the acceptor side limitation or the oxidation level of the P700. Secondly, investigate on the ability to rescue *flva/flvb* KO phenotype by the single over-expression of FLVB gene. Thirdly, perform a comparison between the oeFlvA-FlvB lines and the oeFlvA-2A-FlvB lines, to evaluate the influence of the presence of the 2A peptide at the C-terminal of FlvA. To obtain the necessary data for the screening, the Dual-PAM instrument and the PAM-imaging instrument have been used in parallels with molecular analysis.

2 Materials and methods

2.1 Physcomitrium patens strains

To perform all the experiment, the "Gransden" WT strain has been used as reference strain, from which different mutants have been generated. The *flva/b* KO strain has been previously produced in laboratory, starting from a *P. patens* strain stably mutated for *FlvA*. FABOE lines (oeFlvA-2A-FlvB) have been obtained through the transformation of *flva/b* KO recipient line with a construct, homologous to the one described in Yamamoto et al. 2016 (**Figure 2.1**) composed by a self-cleaved 2A peptide of the foot-and-mouth disease virus sandwiched between the two Flv genes. The latter, transcribed from a single 35S promoter, allow the expression of the two proteins in stochiometric amounts, letting the formation of an active hetero oligomer (Yamamoto et al. 2016) (**Figure 2.1**). The overexpressing *FlvA-FlvB* lines (oeFlvA-FlvB) were instead obtained from a co-transformation of the plasmids pMAK1_FLVA and pT10G_FLVB into *flva/b* KO.

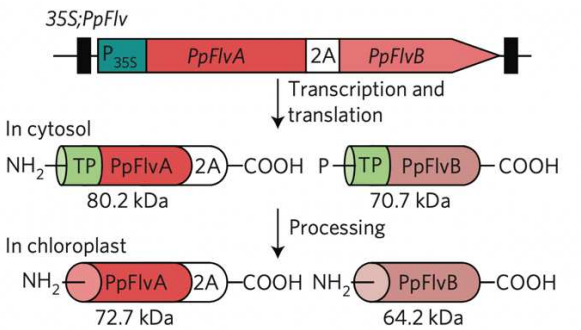

***Figure 2.1 ((Yamamoto et al. 2016)**: A DNA construct for PpFlv expression in Arabidopsis. In the cytosol, two Flv precursors are generated by ribosomal skipping at the last proline residue in the 2A peptide during translational elongation. In chloroplasts, the precursors are matured by the processing of transit peptide (TP). Predicted molecular masses of proteins are indicated.*

2.2 Physcomitrium patens solid cultures

To perform the experiments, *Physcomitrium patens* lines were homogenized with a blender in 10ml of sterile water. To ensure the proper growth, approximately 1.5 mL of this solution was poured onto a Petri dish containing solid medium (either minimal ($PpNO_3$) or enriched ($PpNH_4$), as described in **Table 2.2**), previously covered with a moist cellophane filter. This last, prevent the

homogenized *P. patens* from developing roots anchored to the medium, ensuring easier collection of moss samples from the plate.
Based on the type of medium, $PpNH_4$ plates were sealed completely with parafilm or partially in the case of $PpNO_3$. Respectively, lines were collected after one week or 10 days cultivated in a 24°C growth chamber, with a photoperiod of 16 hours of light / 8 hours of darkness and light intensity of 50µmol photons m^{-1} s^{-1}.

Table 2.2

Media composition		
Compound	**$PpNO_3$**	**$PpNH_4$**
$MgSO_4 \cdot 7H_2O$	0,25 g/L	0,25 g/L
$Ca(NO_3)_2 \cdot 4H_2O$	0,25 g/L	0,25 g/L
$FaSO_4 \cdot 7H_2O$	0,0125 g/L	0,0125 g/L
Microelements (1000 X)	1 ml/L	1 ml/L
Phosphate Buffer (1000 X)	1ml/L	1ml/L
Ammonium tartrate	-	500 mg/L
Glucose	-	5 g/L
Agar	8 g/L	7,2 g/L

2.3 Western blot

2.3.1 SOLUBLE PROTEIN EXTRACTION

The collected material from plates is firstly harvested to form a pellet, which is immediately freezed in liquid nitrogen and stored at -80°C. The pellet is the mechanically disrupted, using a pestle. After obtaining a homogeneous viscous green solution, 100 or 150µl (depending on the initial material amount) of SB 3X + DTT are added. While the Sample Buffer (SB) contains zwitterionic detergents (neutral charge) that solubilize the extracted proteins, the DTT is a denaturing agent that prevents the folding and functioning of proteins (composition reported in **Table 2.3.1a**). To separate proteins in solution from cellular debris, the material obtained from the mechanical destruction is centrifugated at 13000g for 10 minutes and the supernatant is transferred in a new Eppendorf tube. For the chlorophyll quantification, 2µl of supernatant are diluted in 68µl of acetone 80% and then mixed with the vortex. The latter solution is then poured into a quartz cuvette, ready to be analysed at the spectrophotometer (Cary

Series UV-Vis, Agilent Technologies). To determinate the chlorophyll concentration, the absorption values of interest are at the wavelengths 750, 663, and 645 nm and the following formula is used:

$$[Chl]\left(\frac{\mu g}{ml}\right) = \{20.20 \cdot [OD(645) - OD(750)] + 8.02 \cdot [OD(663) - OD(750)]\} \times dil.factor\ (ml)$$

The protein extracts obtained in the previous steps were denatured with a minute of incubation at 100°C. The obtained protein extracts are the loaded on the gel according to the chlorophyll content. Each sample was then brought to the final volume by adding SB 1x as needed.

2.3.2 ACRYLAMIDE GEL PREPARATION

The western blot technique allows to separate proteins based on their molecular weight in a 12% acrylamide gel. The latter is composed by two phases: a stacking portion, in which wells (built with a proper comb) allow to load the sample, and a running portion, where the protein separation takes place. In both cases, the gel is prepared with Acrylamide 40%, SDS 10%, to charge homogeneously charge proteins and let them migrate based just on their molecular weight, mQ water, TEMED and Aps for the polymerization, and finally Tris-HCl. This last component changes depending on the phase of the gel: the Tris-HCl pH8.3 3M is used for the running portion, while the Tris-HCl pH6.8 0.313M is used for the stacking portion (**Table 2.3.2b**). Ultimately, gels are assembled in a box containing Running Buffer (**Table 2.3.2c**)

2.3.3 PROTEIN MIGRATION AND MEMBRANE TRANFER

To perform the protein migration through electrophoresis, acrylamide gels are assembled on a suitable support and soaked into an electrophoresis box filled of Running Buffer, as mentioned in the previous chapter. Samples are loaded into wells, with a final volume that depend on the concentration of the extracts. Proteins migrate in the stacking gel thanks to a constant voltage (40V for 10 minutes) and in the running gel thanks to 80V constant voltage.
The protein transfer from the gel to the nitro cellulose membrane is also achieved using current. The gels are sandwiched with the membrane into a

proper support, flanked by one sponge and two waterman paper on each side. The final composition is soaked into a box filled of Transfer Buffer (**Table 2.3.3d**) with the membrane toward the anode (+), to allow negatively charged proteins to migrate from the gel to the pre-wet membrane. The transfer occurs with a constant voltage of 100V for 1 hour.

2.3.4 MEMBRANE TREATMENT AND ANTIBODY IBRIDIZATION

Immediately after the protein transfer, the membrane is stained with red Ponceau for few minutes to check the transfer quality and the correct protein migration. The membrane is then washed with distillate water to remove the staining and cut based on the molecular weight of the proteins of interest.
To avoid non-specific hybridization of the antibody, the membrane is immersed into 10% dry milk solved in TBS for 1 hour in agitation at room temperature (RT), followed by washes steps with TBS (3 fast washes and 3 washes of 10 minutes each). Primary antibodies are diluted in TTBS based on the required concentration (**Table 2.3.4e**) and must be incubated with the proper membrane fraction for 2 hours at RT or overnight at 4°C. Again, 3 fast washes and 3 washes of 10 minutes each are needed to eliminate the unbound material.
On the primary antibody an epitope is always present, and it is able to recognize the secondary antibody (α-Rabbit or α-Mouse, depending on the first antibody). This last is prepared *de novo* for each experiment with a dilution of 1:5000 in TTBS. For the band visualization, membranes are soaked into BCIP and NBT (33 and 66,6µl).

Table 2.3.1a

Sample buffer	
Composition	**Concentration (3X)**
Tris-HCl pH 6.8	125mM
Glycerol	30%
SDS	9%
DTT	100mM

Table 2.3.2b

Acrylamide 12%		
Composition	**Stacking gel 1X [ml]**	**Running gel 1x [ml]**
Acrylamide 40%	2	0.333
Tris-HCl 3M pH8.8	0.827	-
Tris-HCl 0.313M pH6.8	-	1.25
SDS 10%	0.067	0.033
milliQ water	3.773	1.716
APS 10%	0.02	0.017
TEMED	0.0133	0.012

Table 2.3.2c

Running Buffer	
Tris pH8.3	250mM
Glicina	1.92 M
SDS	1%

Table 2.3.3d

Transfer Buffer	
Tris pH8.3	20mM
Glycine	152mM
Methanol	20%

Table 2.3.4e

Antibody dilution	
Antibody	**Dilution**
α-FlvA	1:500
α-FlvB	1:500
α-D2	1:500
α-PSBS	1:500

2.4 PAM imaging analysis

2.4.1 FLUORESCENCE PROTOCOL

Light energy absorbed by chlorophyll molecules can drive photosynthesis (photochemistry), be dissipated as heat, or be re-emitted as light (fluorescence) (**Figure 2.4.1a**). These three processes do not exist in isolation but rather in competition with each other. Assuming that the variation in the fluorescence signal arise from PSII only and, thus, ignoring the emission from PSI, chlorophyll fluorescence analysis allow to quantify the energy dissipation of chlorophyll as an indirect measure of photosynthetic efficiency (Murchie e Lawson 2013).
The measurements are performed in a dark-adapted state. This allow all the PSII reaction centers to go from a close to an open state. In the open state, the reaction center chlorophylls are reduced and the primary electron acceptors, Q_A and Q_B, together with all the electron transport chain components, are oxidized. When the measuring light is switched on, the intensity is too low to induce electron transport through PSII, but high enough to elicit a minimum value for chlorophyll fluorescence, recorded as F_0 (**Figure 2.4.1b**).

The application of a saturating pulse (SP) to a dark-adapted sample induces a maximum value of fluorescence (F_m) emitted by antenna proteins pigments which cannot transfer the excitation energy to the reaction centre which are in the close state. In a healthy non-stressed plant, there is no NPQ because the material has been fully dark adapted; therefore, the maximal possible value for fluorescence, F_m, is recorded. The difference between F_0 and F_m is the variable fluorescence, F_v. It has been shown that F_v/F_m gives a robust indicator of the maximum quantum yield of PSII chemistry. For unstressed samples, this value is highly consistent, with values of ~0.79, and correlates to the maximum quantum yield of photosynthesis. The existence of any type of 'stress' that results in inactivation damage of PSII (photoinhibition) or the induction of sustained quenching, results in a lower difference between F_0 and F_m and lower value of F_v/F_m.

When the actinic light (AL) is switched on, the fluorescence emission is lower compared to the one recorded in the dark state, due to the competition with the photochemistry events and the NPQ. In stressed samples, this value is lower respect to the stressed ones and allow to select functional clones. During the AL exposure, at each SP a F_m' is recorded, allowing to determinate Y(II) and NPQ (Murchie e Lawson 2013).

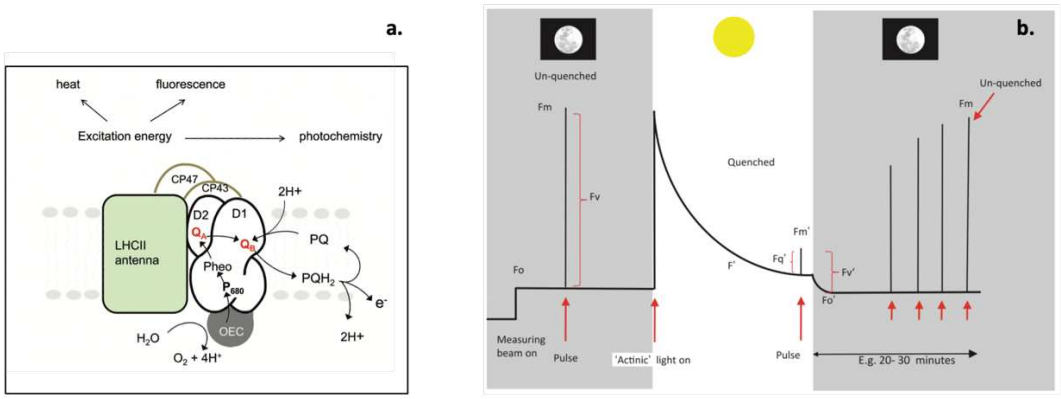

***Figure 2.4.1 (Murchie e Lawson 2013)**: A simplified depiction of events in PSII, leading to the identification of key parameters in fluorescence analysis. **a.** Schematic figure showing electron transport within the PSII reaction centre complex. Energy absorbed by chlorophyll within the light-harvesting complex can be dissipated via different ways. **b.** A stylized fluorescence trace of a typical experiment using dark-adapted leaf material to measure photochemical and non-photochemical parameters. This would be typical of an induction at high irradiance of ≥500 µmol $m^{-2}s^{-1}$. More explanation is given in the text.*

2.5 Dual-PAM

2.5.1 DUAL-PAM INSTRUMENT

In contrast to PSII, in PSI the fluorescence yield at room temperature is independent of the state of the reaction center hence, it cannot serve as an indicator of photochemical efficiency. For this reason, using a modified emitted-detector unit, it's possible to measure the redox state of P700 (the reaction canter chlorophyll of PSI), via its absorbance change in the near-infrared. The signal is minimal when P700 is completely reduced in darkness and increases upon light-driven oxidation (**Figure 2.5.1**) (Klughammer e Schreiber 2008).
In order to distinguish whether PSI centers chlorophylls (P700) are in a reduced or oxidized state, a Saturating Pulse method has been set up. The complete oxidation of P700 is induced by a Saturating Pulse (SP) in presence of Far-Red (FR) light and the resulting signal is denoted as Pm. On the contrary, complete reduction of the reaction center chlorophyll of PSI is recorded when the SP and the FR light are turned off, providing the zero P700 signal denoted by Po. All P700 signals changes occur between Pm and Po. When the actinic light (AL) is activated, a portion of P700 called donor-side limited closed center ($P700^+$, A) is oxidized and it's denoted as P. In this moment, the signal change induced by a saturation pulse (SP) corresponds to the oxidation of the active fraction of P700 (open centers P700, A), and the maximum P700 signal is represented as Pm'. The fraction that remains unoxidized (acceptor-side limited closed centers P700, A^-) is the difference between Pm and Pm' (**Figure 2.5.1**) (Klughammer e Schreiber 2008)
In the **Table 2.5.1** the state of PSI reaction center and the correspondent donor or acceptor side limitation level are highlighted.

Table 2.5.1

$P700^+$ A (closed)	Y(I) = 0	Y(ND) = 1	Y(NA) = 0
P700 A (open)	Y(I) = 1	Y(ND) = 0	Y(NA) = 0
P700 A^- (closed)	Y(I) = 0	Y(ND) = 0	Y(NA) = 1

DUAL-PAM SETTINGS

To perform the physiological analysis, all the available *P. patens* lines described in the first section have been analysed with DUAL-PAM. The plants were growth in a $PpNO_3$ solid medium for 10 days before the analysis.
To set the instrument, the first step is to pre-heated the PML led and to dark-acclimatise the sample for almost 30 minutes. Then, the procedure consists in withdraw a small amount of sample and place it on the top of a pre-wet fiberglass filter. For both protocols used, at the very beginning of each experiment, the sample has been submitted to a far-red light (FR) for 15 seconds in order to completely oxidise the P700 prior Pm determination.
A protocol named "Induction and Recovery" has been used to investigate on the effect of the accumulation of FLVs, both in the dark-to-light transition and at steady state. It consists in 8 minutes of actinic light (AL), with a SP every 30 seconds, followed by 8 minutes of dark, with a SP at incremental intervals. The intensity of the AL was set at 500µmol photons $m^{-1}s^{-1}$.
To examinate the effect of the possible photodamage due to overexpression of FLVs, a "Fluctuating protocol" has been set up. For the entire duration of the experiment, the lines were submitted to 1 minute of high light (800µmol photons $m^{-1}s^{-1}$), followed by 4 minutes of dark. The Pm was recorded at the beginning, every 20 minutes and at the end of the protocol. For a better description of these experiment and the data analysis, see the results.

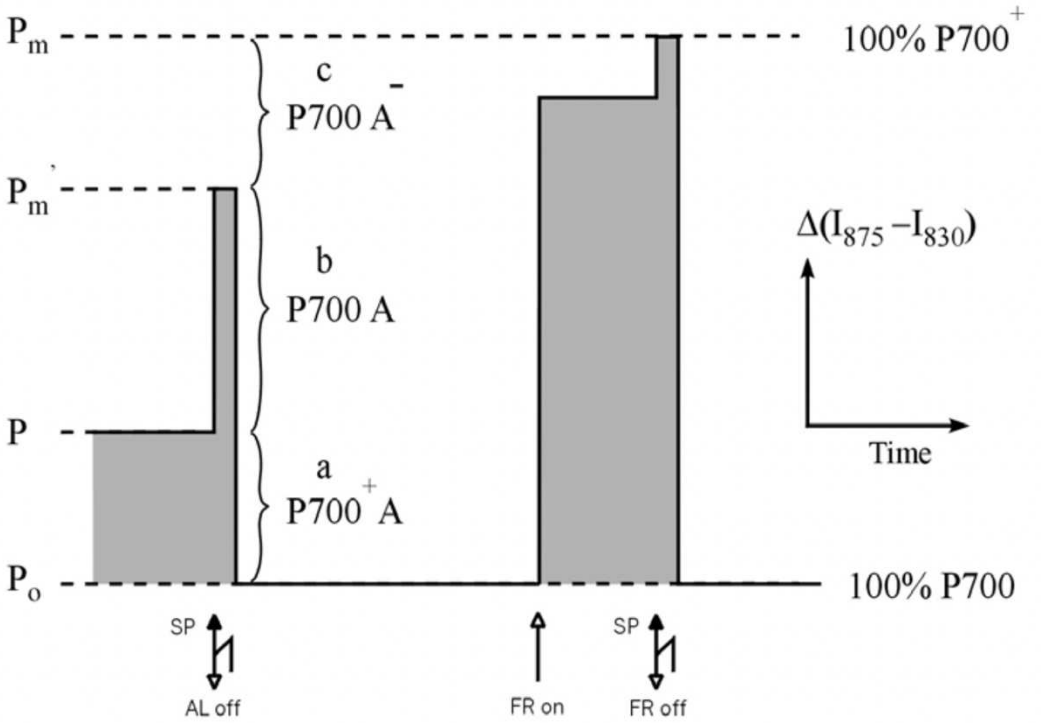

Figure 2.5.1 (Klughammer e Schreiber 2008)*: Principle of Saturation Pulse method for determination of efficiency of energy conversion in PS I (modified from Klughammer and Schreiber, 1994). P700 is measured in the dual-wavelength mode (difference of intensities of 875 nm and 830 nm pulse-modulated measuring light reaching photodetector). P700 oxidation is characterized by a positive signal change. Complete P700 oxidation is induced by a Saturation Pulse (SP) in the presence of Far-Red (FR) light, with the maximal P700 signal denoted by Pm. Complete reduction is induced after the SP and cessation of FR-illumination, with the zero P700 signal denoted by Po. In the presence of Actinic Light (AL) a fraction a (donor-side limited closed centers P700+A) is oxidized by the AL resulting in an intermediate P700 signal denoted by P. In this state the SP-induced signal change corresponds to the oxidation of the active fraction b (open centers P700 A), with the maximal P700 signal being denoted by Pm'. The fraction c (acceptor-side limited closed centers P700 A-) that cannot be oxidized, corresponds to the difference between Pm and Pm'.*

2.6 Spot Test

To perform a Spot Test, P. patens lines are cultured in a minimum media for 10 days. The whole experiment last one months and small pieces of moss tissue are let grow in a $PpNO_3$ plates without the filter. For each strain, 3 spots are created (**Figure 2.6**). The latter consist in a homogeneous accumulation of the material in a circular area with a diameter of about 3mm. Once the plates are prepared, they are stored for one day under Control Light (CL) with a constant intensity of 50µmol photons $m^{-1}s^{-1}$, in order to allow the plant recovery from the stress. The second day, the Fv/Fm is recorded at the PAM-imaging (after 30 minutes of incubation) and a photo is obtained with a scanner. At this point, plates are

ready to be incubated in different light conditions. In particular: control Light (50µmol photons $m^{-1}s^{-1}$), High Light (500µmol photons $m^{-1}s^{-1}$), Fluctuating Light (1-minute 800µmol photons $m^{-1}s^{-1}$ and 5 minutes 25µmol photons $m^{-1}s^{-1}$). To trace the plant efficiency and growth, the Fv/Fm and the photo are repeated at day 7, 14, 21 and 28. Spot dimensions are analyzed with ImageJ program, while the Fv/Fv with data analysis programs.

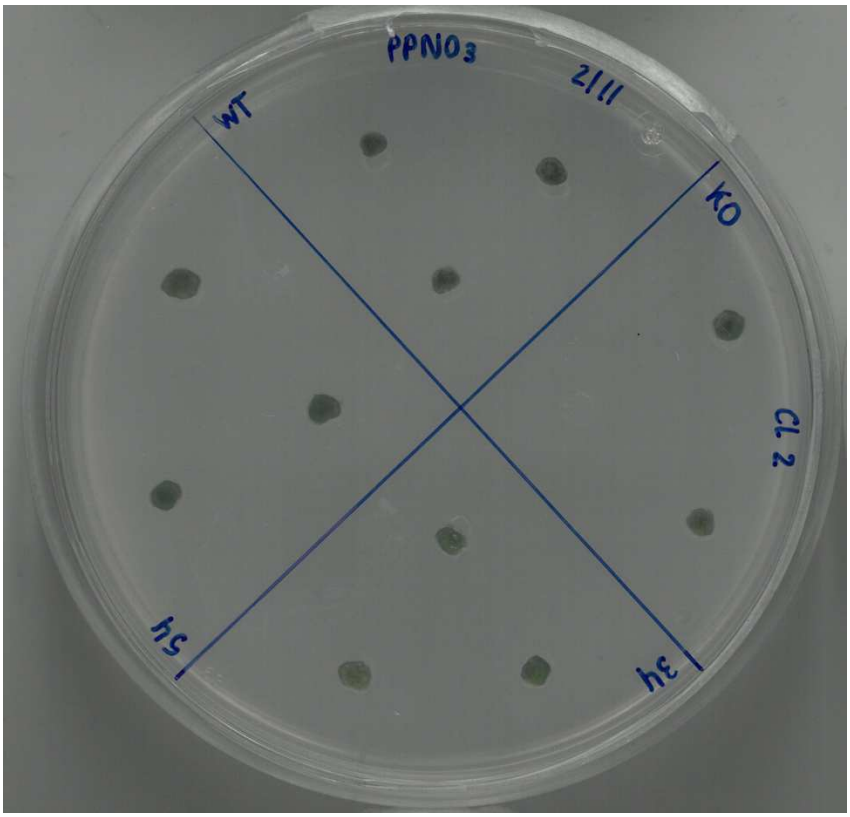

***Figure 2.6**: Photo example of a spot test plate. For each analyzed line, 3 technical replicas are reported. Spots have a diameter of about 3mm and they grow in a minimum medium.*

3 Results

3.1 The fluorescence as a screening method for *Physcomitrium patens* lines

The FlvA-FlvB lines, resulting from the co-transformation of pMAK1_FLVA and pT10G_FLVB plasmids into the flva/flvb knockout (KO) strain, as detailed in the materials and methods section, underwent an initial screening analysis. To identify successfully transformed lines, clones that had survived the prior antibiotic selection, were subjected to fluorescence analysis using the PAM imaging instrument (**Figure 3.1a**). The screening protocol exploits the principle that the excitation energy in photosystems can be dissipated by previously described competing pathways (photochemistry, heat or fluorescence).
As elucidated in the introduction, Flavodiiron proteins (FLVs) function downstream of photosystem I and play a crucial role in the dark-to-light transition (Alboresi et al. 2019). Consequently, their absence diminishes electron transport and associated photochemistry, leading to an increase in fluorescence. Once the actinic light is switched and the saturating pulse occur, the wild-type line (WT) exhibits a fluorescence level of approximately 0.5 (**Figure 3.1b**), serving as an arbitrary threshold for discriminating clones expressing FLVs functionally from others.
Results from the fluorescence analysis reveal that, during the dark-to-light transition, FlvA-FlvB lines segregate into two groups (**Figure 3.1c**): one group with values resembling the WT (fluorescence ≤ 0.5), and another exhibiting a behaviour more similar to the KO (fluorescence > 0.5).
Nevertheless, PAM-imaging analysis is an empirical observation-based method, providing indirect information about the expression and proper function of FLVs. Consequently, clones that survived antibiotic selection and exhibited fluorescence levels either < 0.5 or > 0.5 were collected, suspended in 10 mL of sterile water, or frozen at -80°C for subsequent protein profile analysis. Specifically, Western Blots were conducted to confirm the effective expression of both FLVs in lines characterized by fluorescence levels ≤ 0.5 and to ascertain the presence or absence of these proteins in lines that grew during antibiotic selection but showed fluorescence levels > 0.5.

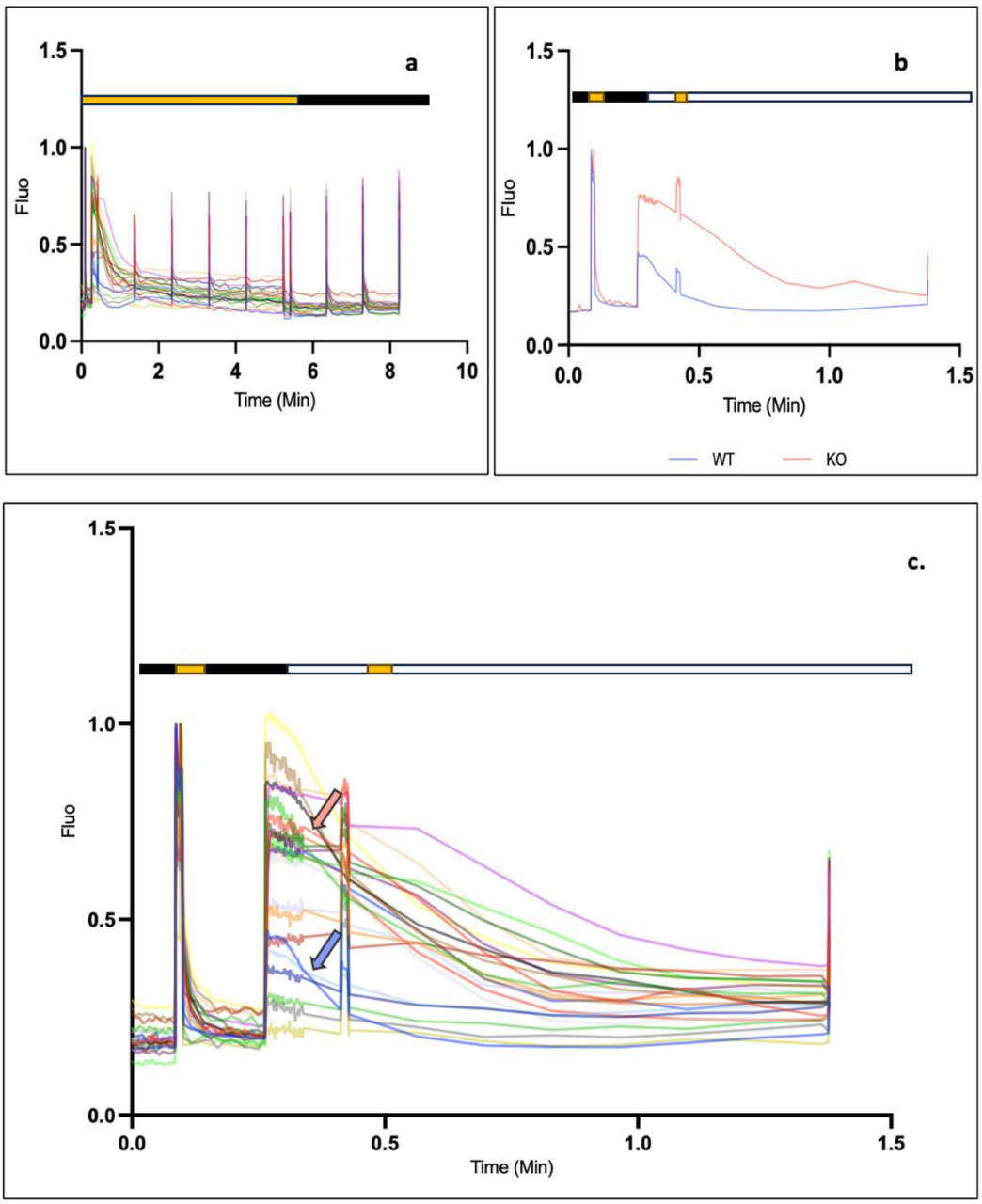

*F**igure 3.1:** Fluorescence analysis at PAM imaging (≪Slow Kinetic≫ protocol: 5'' dark – SP – 10''dark – 300''AL with a SP every 45'') of flva/flvb KO transformed with pMAK1_FLVA and pT10G_FLVB plasmids and growth in $PpNO_3$ for 7 days. **a.** The level of florescence is reported for all the lines that survived at the antibiotic selection. Each peach corresponds to a SP. **b.** Fluorescence level for WT and KO lines. **c.** Focus on the first minute of the ≪Slow Kinetic≫ protocol. The red arrow indicates the KO, while the blue one indicates the WT. All the clones locate close to one or the other, allowing the formation of two groups: clones with fluorescence <0.5 and clones with fluorescence >0.5.*

3.2 Molecular analysis to investigate on the expression of FlvA and FlvB in oeFlvA-FlvB lines

In accordance with the previously paragraph, the verification of effective FLVs expression involved the performance of Western Blot analysis. All lines subjected to the PAM-imaging fluorescence protocol were loaded in the 40% acrylamide gel with a chlorophyll quantity of 3µg, except for the wild-type (WT) and knockout (KO) lines, which were loaded with a 6µg chlorophyll quantity too. Subsequent to protein transfer, membranes were incubated with a primary antibody against either FlvA or FlvB. To assess the potential impact of FLVs on the photosynthetic apparatus, FlVs were compared with two constitutively expressed proteins, D2 and PsbS, to investigate potential alterations in the degradation levels of D2 and PsbS in lines overexpressing FLVs. No detectable differences were observed.

Figure 3.2 reports the results of both Ponceau red staining and immunoblotting. Ponceau red staining was employed to confirm the uniform loading of samples. Lines #4, #13, #18, and #27 are indicative of "WT-like" clones, as evidenced in Figure 3.2a, b, e, and f, wherein the intensity of FlvA and FlvB bands are similar to the ones observed in the WT when loaded with equivalent chlorophyll quantities. Conversely, lines #8, #26, #30, #46, and #54 exhibit bands with higher density compared to the WT, indicating overexpression of both FlvA and FlvB. Consequently, these lines are designated as "oeFlvA-FlvB lines."

Upon closer examination, certain lines, such as #7, #17, and #34, mostly express the FlvB protein (**Figure 3.2a., b, c,** and **d**) and are denoted as "oeFlvB lines," while others (#6, #40, and #41) exclusively express FlvA, but the background noise must be considered. The remaining lines exhibit minimal or absent FLVs expression.

To explore the correlation between FlvA and FlvB, the optical density of immunoblot bands for both proteins was quantified using ImageJ software. Normalization for the WT of the same gel was conducted for each clone, and the obtained data were plotted in the histogram presented in **Figure 3.2g**. Given that FLVs work as a heterodimer (Alboresi et al. 2019), a Linear Regression analysis was performed using GraphPad software. The resulting R2 value of 0.3628 suggests a positive regression between FlvA and FlvB. However, due to the

limited number of replicates, this observation cannot be confirmed (**Figure 3.2h**).

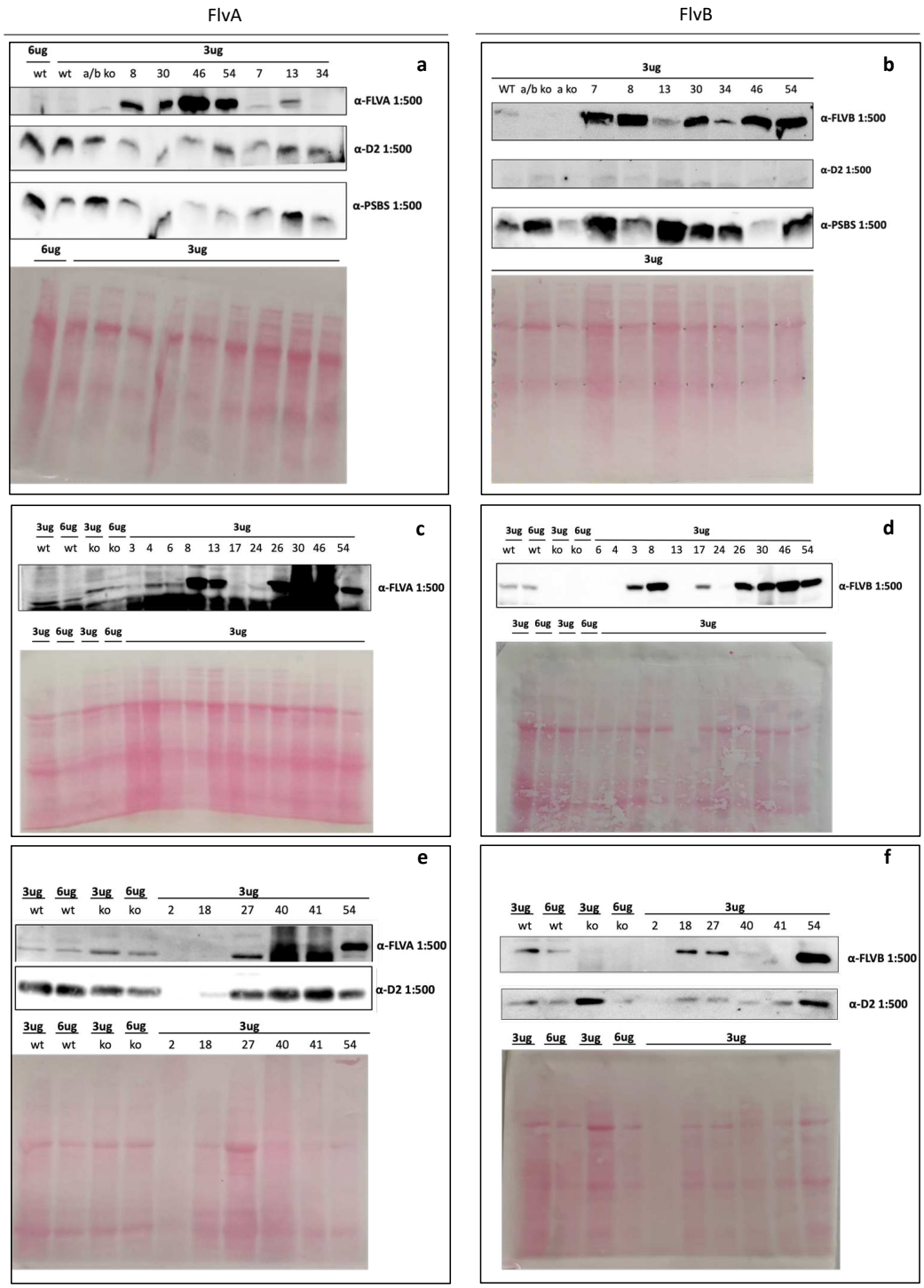

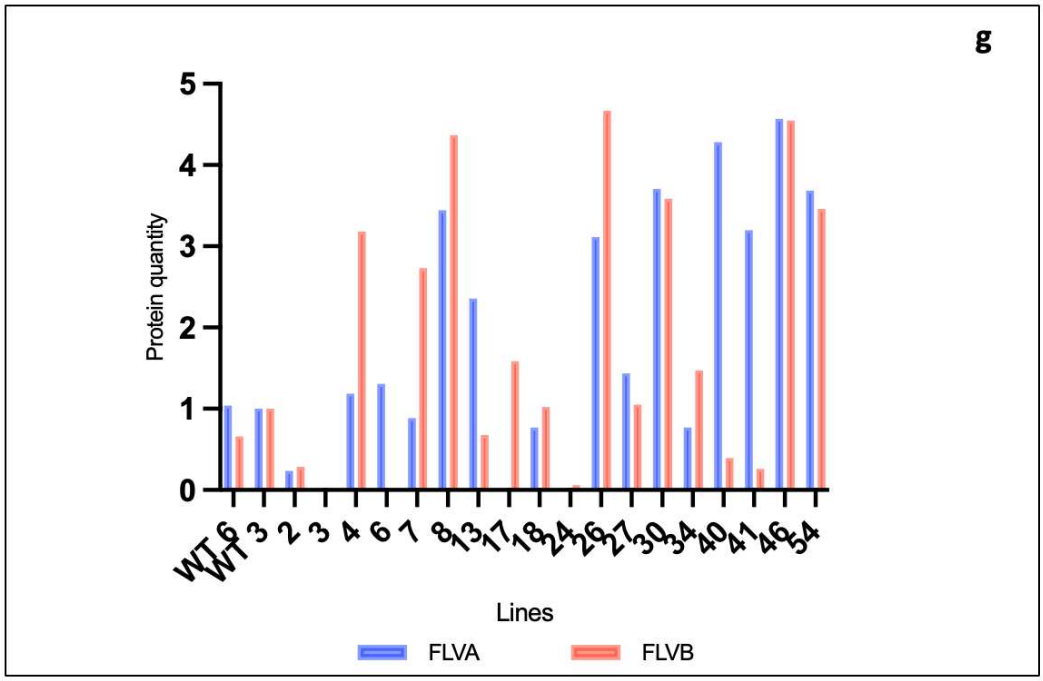

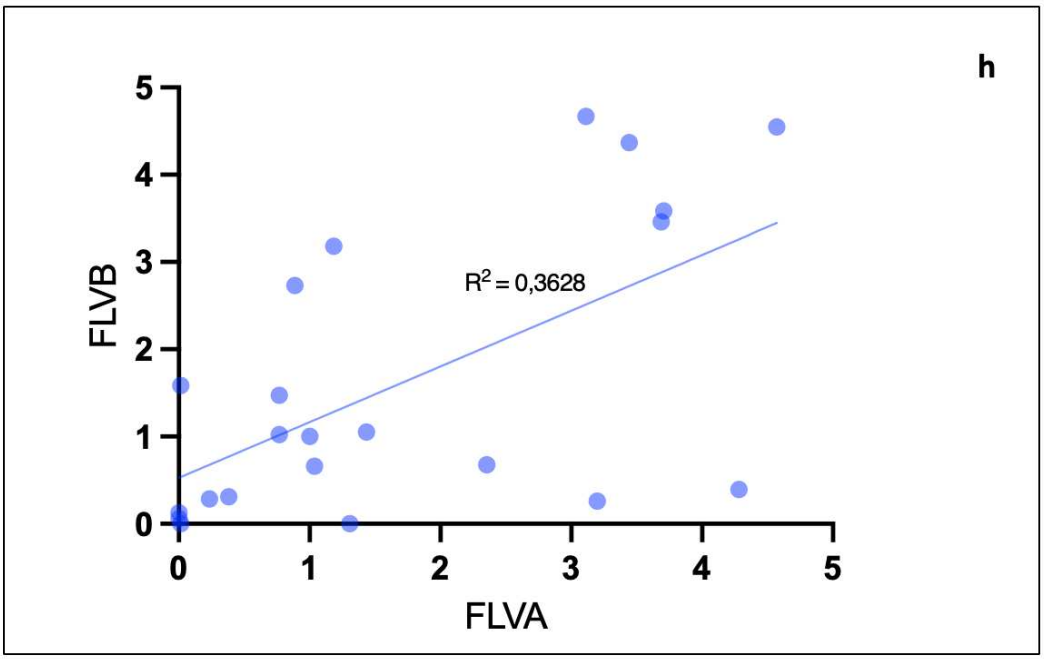

***Figure 3.2**: **a-f.** Western Blots of proteins mechanically extracted with SB 3x+DTT. FlvA-2A-FlvB lines, growth in $PpNO_3$ culture for 10 days, are compared with positive and negative control, WT and KO respectively. For these last, two different amounts of chlorophylls were loaded (3ug and 6ug), while for all the FlvA-2A-FlvB lines 3ug were used. Membranes were firstly incubated with primary antibodies (α-FlvA, αFlvB, $\alpha D2$ and αPsbS) and then hybridized with a secondary antibody α-Rabbit. Band visualization after the addition of BCIP and NBT (33 and 66,6µl). **g.** Histogram of the relative expression of FlVs for all the clones previously screened with PAM-imaging instrument. Data were obtained after the quantification of the FlvA (in blue) and FlvB (in red) optical density of the immunoblot bands with ImageJ program. The resulting value of each clone has been normalized for the WT of the same loading gel. **h.** Linear Regression between FlvA and FlvB optical density bands data coming from the molecular analysis of the lines selected for the screening. R^2=0,3628*

3.3 The effect of the accumulation of FlvA and FlvB on the photosynthetic parameters

Flavodiiron proteins (FLVs) play a crucial role downstream of photosystem I, avoiding the overreduction of the electron transport chain, particularly under stress light conditions (Alboresi, Storti, e Morosinotto 2019). To explore the impact of the accumulation of both FLVs, specific physiological parameters were assessed using the DUAL-PAM instrument. The Induction and Recovery protocol has been applied, with an actinic light intensity set at 500µmol photons $m^{-1}s^{-1}$ (saturating light). Clones identified as overexpressing lines through prior molecular analysis (#8, #26, #30, #46, and #54) were selected for the research. Firstly, a focus on the acceptor side limitation (Y(NA)) parameter during the dark-to-light transition was done (**Figure 3.3**). Although the overall kinetics between the positive and negative controls were similar, a noteworthy difference was observed at the initial point of Y(NA) (**Figure 3.3a, b**). Specifically, the first point of Y(NA) in oeFlvA-FlvB lines (averaged from #8, #26, #30, #46, and #54) exhibited a significant rescue of the phenotype compared to the negative control line, *flva/flvb* KO. Remarkably, the Y(NA) value at the first point of the kinetic in oeFlvA-FlvB lines was even lower than that in the WT (**Figure 3.3a, b**).
Beside the Y(NA) parameter, also the donor side limitation (Y(ND)) parameter was analyzed (**Figure 3.3c, d**). As reported in (Alboresi et al. 2019), the Y(ND) results high in FLVs expressing lines, oppositely to what it's observe with the Y(NA). As expected, the fist point of the YND) kinetic results low in the *flva/flvb* KO, while it assumes higher values in the WT and in the oeFlvA-FlvB lines, demonstrating a significative difference between them. Except for the first point of Y(ND) kinetic, no significative differences have been detected during the entire duration of Y(D) kinetic (**Figure 3.3c**)
To further probe the effects of FLV overexpression, additional physiological parameters were analyzed. Among these, Y(I), NPQ, and Y(II) kinetics are presented in **Figure 3.3e, f, g**. Statistical analysis revealed no significant differences, between the compared lines.

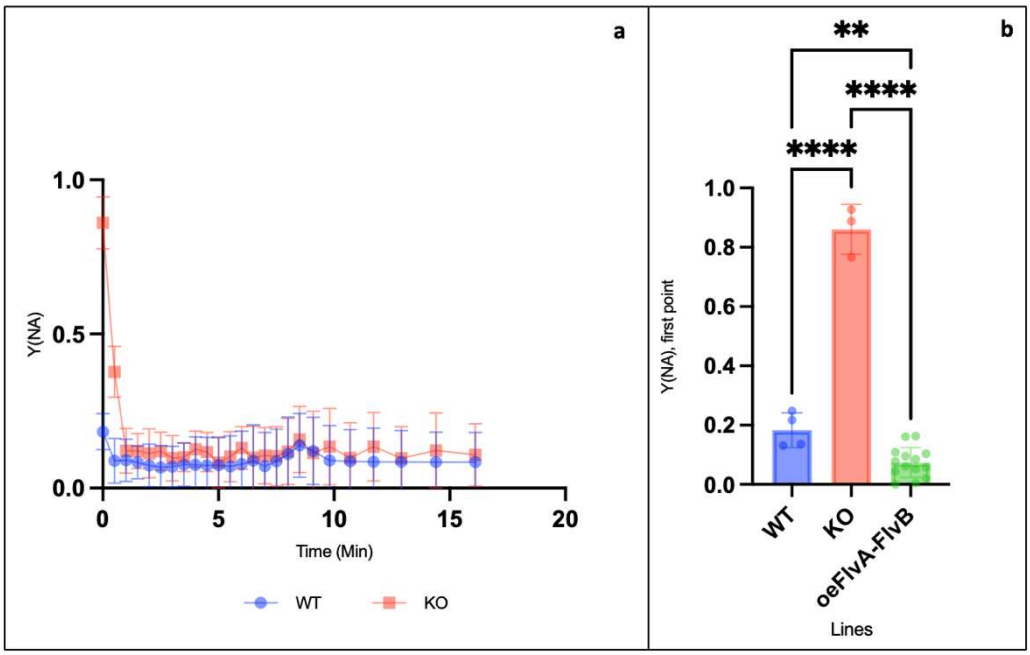
a
1.0
0.5
0.0
Y(NA)
0
5
10
15
20
Time (Min)
WT
KO
b
**
****
****
1.0
0.8
0.6
0.4
0.2
0.0
Y(NA), first point
WT
KO
oeFlvA-FlvB
Lines

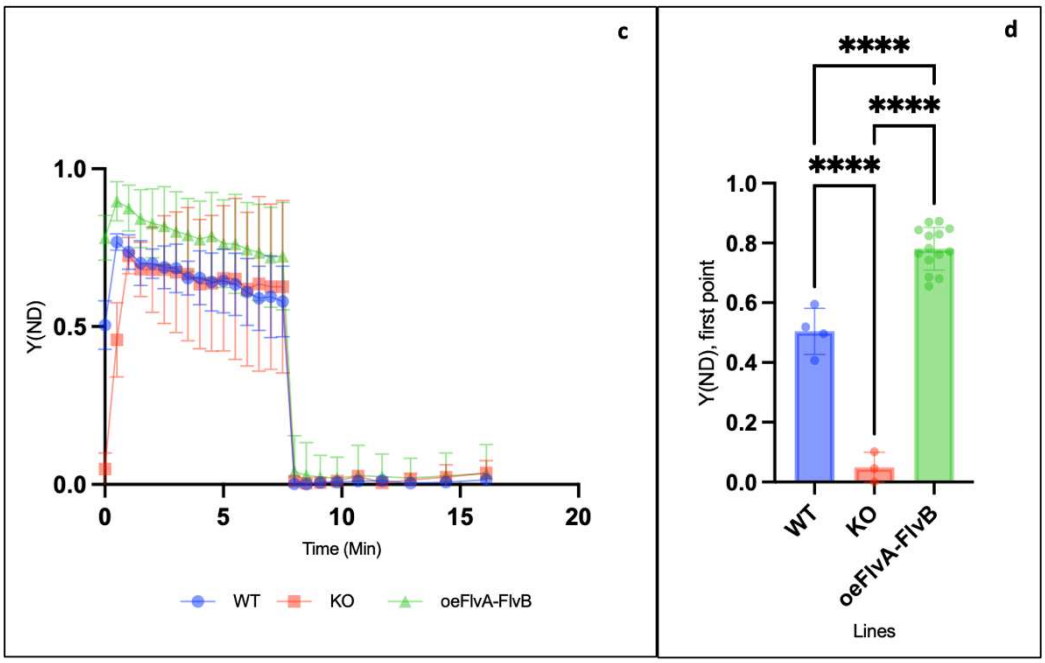
c
1.0
0.5
0.0
Y(ND)
0
5
10
15
20
Time (Min)
WT
KO
oeFlvA-FlvB
d
****
****
****
1.0
0.8
0.6
0.4
0.2
0.0
Y(ND), first point
WT
KO
oeFlvA-FlvB
Lines

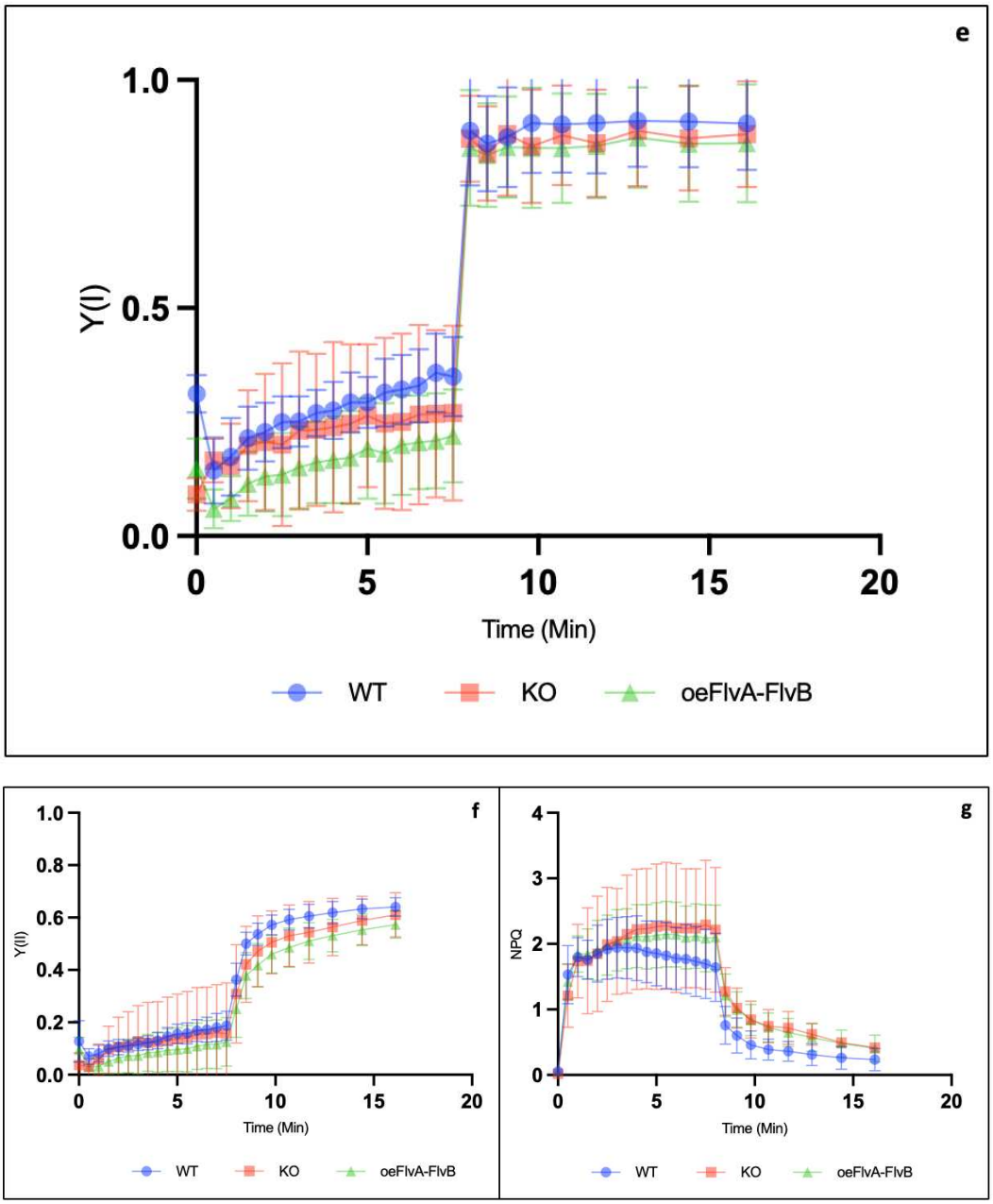

***Figure 3.3**: DUAL-PAM analysis performed on WT line (blue), KO line (red) and oeFlvA-FlvB lines (green). The "Induction&Recovery" protocol (8 minutes of actinic light (AL), with a SP every 30 seconds, followed by 8 minutes of dark, with a SP at incremental intervals) is exploited. The intensity of the AL was set at 500µmol photons $m^{-1}s^{-1}$. **a.** Y(NA) kinetics are reported for both positive (WT) and negative (KO) controls. A focus is put on the first point of the kinetic of Y(NA), which appear significative difference between the two lines (one-way ANOVA, P<0.0001). **b.** Histogram of the first point of Y(NA) for WT, KO and oeFlvA-FlvB lines (#8, #26, #30, #46 and #54). The statistical analysis reveals a significative difference of oeFlvA-FlvB lines compared with the WT (one-way ANOVA, P<0.0095), and the KO (one-way ANOVA, P<0.0001). **c.** Y(ND) kinetics are reported for positive (WT) and negative (KO) controls and for the oeFlvA-FlvB lines. No significative differences have been detected (one-way ANOVA, P>0.05) **d.** A focus is put on the first point of the kinetic of Y(ND), which appear significative difference between the two control lines (one-way ANOVA, P<0.0001). The relative histogram is reported. The oeFlvA-FlvB lines are significative difference between the KO (one-way ANOVA, P<0.0001) and the WT (one-way ANOVA, P<0.0001). **e.** Y(I) (one-way ANOVA, P>0,05). **f.** Y(II) (one-way ANOVA, P>0,05). **g.** NPQ (one-way ANOVA, P>0,05).*

3.4 The effect of the accumulation of the single FlvB protein on the photosynthetic parameters

As it has been mentioned in the introduction, flavodiiron proteins coding sequences are found in couples (FLVA/FLVB) and, once they are expressed, they work as a heterodimer (Alboresi et al. 2019).
To achieve to the second aim of this work, which is to investigate on the effect of the accumulation of just one of the two FLVs, just FlvB expressing lines (oeFlvB lines) have been analyzed at the DUAL-PAM instrument. Lines of interest (oeFlvB lines), analyzed with the Induction and Recovery protocol, were firstly mediated, and then compared with the two control lines, WT and *flva/flvb* KO respectively. In particular, such as for the previous results, a focus has been put on the acceptor side limitation value (Y(NA)). In **Figure 3.4a**, the kinetic of Y(NA) is reported. No significative difference emerged, except at the first point of the Y(NA) kinetic. As it is possible to appreciate in **Figure 3.4b**, the difference between the WT and the oeFlvB lines result significative, indicating that the expression of just FlvB do not let to the rescue of the phenotype. On the other hand, also the level of difference between oeFlvB lines and the negative control (KO) is significative, suggesting that the expression of just one of the two FLVs could also has a negative impact on the physiological functions.
Analysis regards the Y(NA) parameter, were performed in parallel on the donor side limitation (Y(ND)) parameter (**Figure 3.4**). As explain in (Alboresi et al. 2019), the Y(ND) at the first point is expected to be higher in the WT, while it assumes lower values for the KO. Both the kinetic and the first point of the Y(ND) are reported (**Figure 3.4c** and **3.4d**, respectively). It is possible to appreciate that the two controls are significative difference one with the other. A significative difference is observed also between the WT and the oeFlvB lines, where the latter don't show any difference compared with the KO.
To obtain an overall contest of the effect of the over expression of just FlvB, other physiological parameters (Y(ND), Y(I), NPQ and Y(II)) are reported below in **Figure 3.4e.f.g**. The statistical analysis doesn't reveal significative differences between the two controls (WT and *flva/flvb* KO), and between them and the lines of interest (oeFlvB).

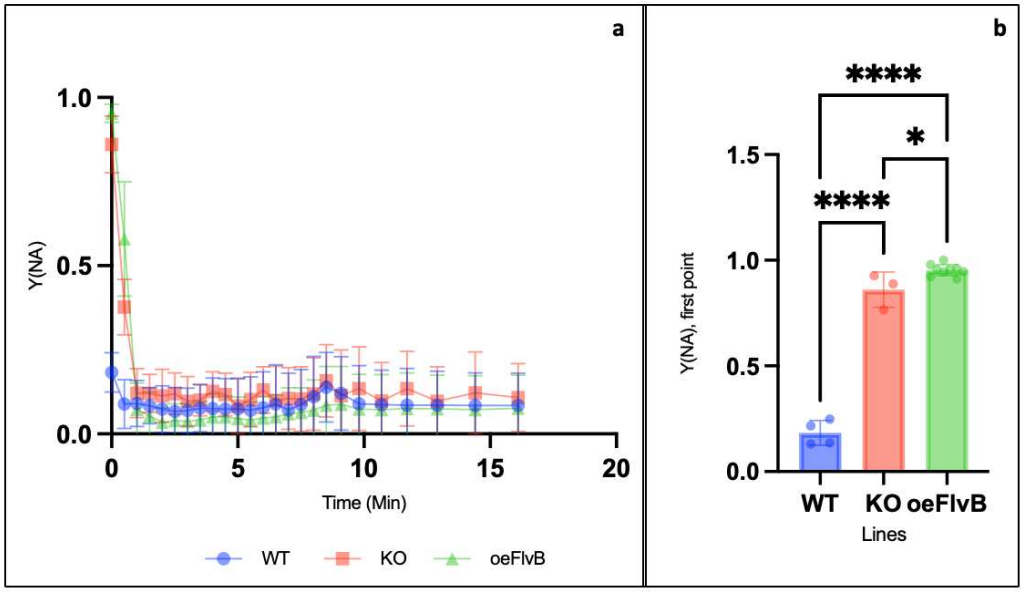
a
1.0
0.5
0.0
Y(NA)
0
5
10
15
20
Time (Min)
WT
KO
oeFlvB
b
****
*
****
1.5
1.0
0.5
0.0
Y(NA), first point
WT
KO
oeFlvB
Lines

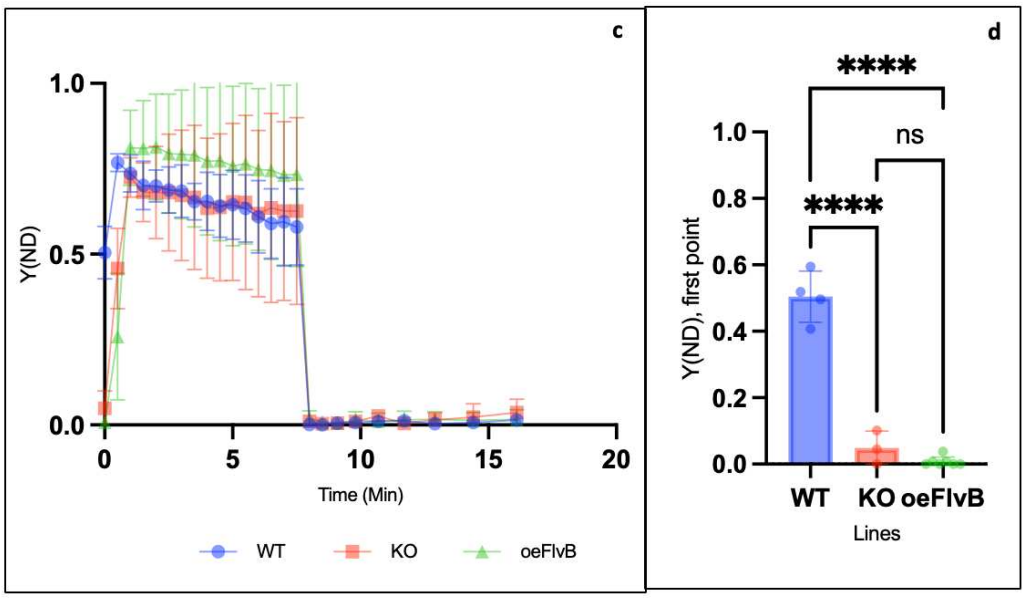
c
1.0
0.5
0.0
Y(ND)
0
5
10
15
20
Time (Min)
WT
KO
oeFlvB
d
****
ns
****
1.0
0.8
0.6
0.4
0.2
0.0
Y(ND), first point
WT
KO
oeFlvB
Lines

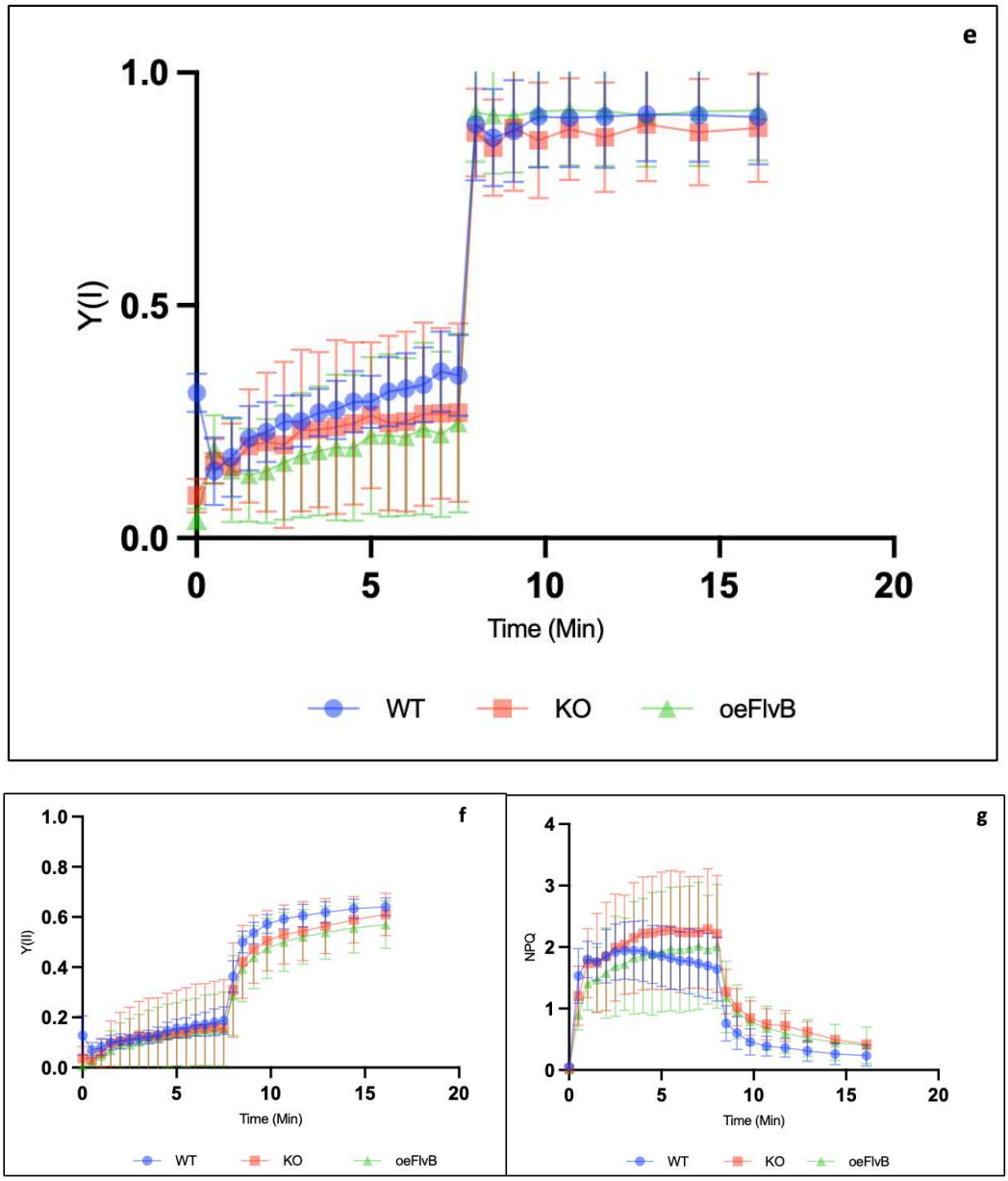

***Figure 3.4**: DUAL-PAM analysis performed on WT line (blue), KO line (red) and oeFlvB lines (green). The "Induction&Recovery" protocol (8 minutes of actinic light (AL), with a SP every 30 seconds, followed by 8 minutes of dark, with a SP at incremental intervals) has been exploited. The intensity of the AL was set at 500µmol photons $m^{-1}s^{-1}$. **a.** Y(NA) kinetics reported for all the lines: WT, KO and the mediated oeFlvB lines (#7, #17 and #34). **b.** Histogram of the first point of Y(NA) for WT, KO and oeFlvB lines (#7, #17 and #34). The statistical analysis reveals a significative difference between the two control lines, WT and KO (one-way ANOVA, P<0.0001) and between the positive control and the oeFlvB lines (one-way ANOVA, P<0.0001). The difference between the KO and the oeFlvB is significative too (one-way ANOVA, P<0.0376). **c.** Y(ND) kinetics are reported for positive (WT) and negative (KO) controls and for the oeFlvB lines. No significative differences have been detected (one-way ANOVA, P>0.05) **d.** A focus is put on the first point of the kinetic of Y(ND), which appear significative difference between the two control lines, WT and KO (one-way ANOVA, P<0.0001). The relative histogram is reported. The oeFlvB lines are not significative difference compared to the KO (one-way ANOVA, P>0.05). On the contrary, if it is compared to the WT, statistical analysis results significative (one-way ANOVA, P<0.0001). **e.** Y(I) (one-way ANOVA, P>0,05). **f.** Y(II) (one-way ANOVA, P>0,05). **g.** NPQ (one-way ANOVA, P>0,05).*

3.5 The impact of the peptide 2A on the physiological functions

As it has been described in “Materials and Methods”, the oeFlvA-2A-FlvB lines are characterized by the presence of a self-cleaved 2A peptide sandwiched between two Flv genes. The latter, transcribed from a single 35S promoter, allow the expression of the two peptides in stochiometric amounts, letting the formation of an active hetero oligomer (Yamamoto et al. 2016).
Previous analysis in the lab highlighted the presence of two groups of clones based on the FLVs expression level: strong oeFlvA-2A-FlvB lines (over expressing at least 10 times more FLVs than the WT) and mild oeFlvA-2A-FlvB lines (expressing only two time more FLVs than the WT).
In order to observe whether the 2A peptide effect protein functioning, the same physiological analysis described for oeFLVA-FLVB lines have been performed on strong and mild oeFlvA-2A-FlvB lines too.

3.5.1 STRONG oeFlvA-2A-FlvB LINES

In our investigation, particular attention was put on the Y(NA) parameter. Although the overall kinetics (**Figure 3.5.1a, b**) where resulting traces overlap, the most notable distinctions were observed at the initial point of Y(NA). In particular, as described in the histogram in **Figure 3.5.1b**, statistical analysis revealed significant differences between the *flva/flvb* KO and both the oeFlvA-FlvB lines and strong oeFlvA-2A-FlvB lines.
Remarkably, no discernible differences were identified between the oeFlvA-FlvB lines and oeFlvA-2A-FlvB lines, suggesting that the presence of the 2A peptide did not exert any significant effect on Y(NA) (**Figure 3.5.1b**).
Analogous analyses related to the Y(NA) parameter were conducted for the donor side limitation (Y(ND)) parameter. Both the kinetic profile and the initial point of Y(ND) are presented in **Figure 3.5.1c** and **Figure 3.5.1d**, respectively. While the WT and *flva/flvb* KO displayed significant differences, no significant distinctions were observed between the oeFlvA-FlvB lines and the strong oeFlvA-2A-FlvB lines.
To further explore the effects of FLV overexpression, additional physiological parameters including Y(I), Y(II), and NPQ kinetics were reported (**Figure 3.5.1e, f, g**). The statistical analysis revealed no significant differences, both between the

two control lines (WT and KO) and between the control lines and the lines overexpressing FLVs (oeFlvA-FlvB and strong oeFlvA-2A-FlvB lines).

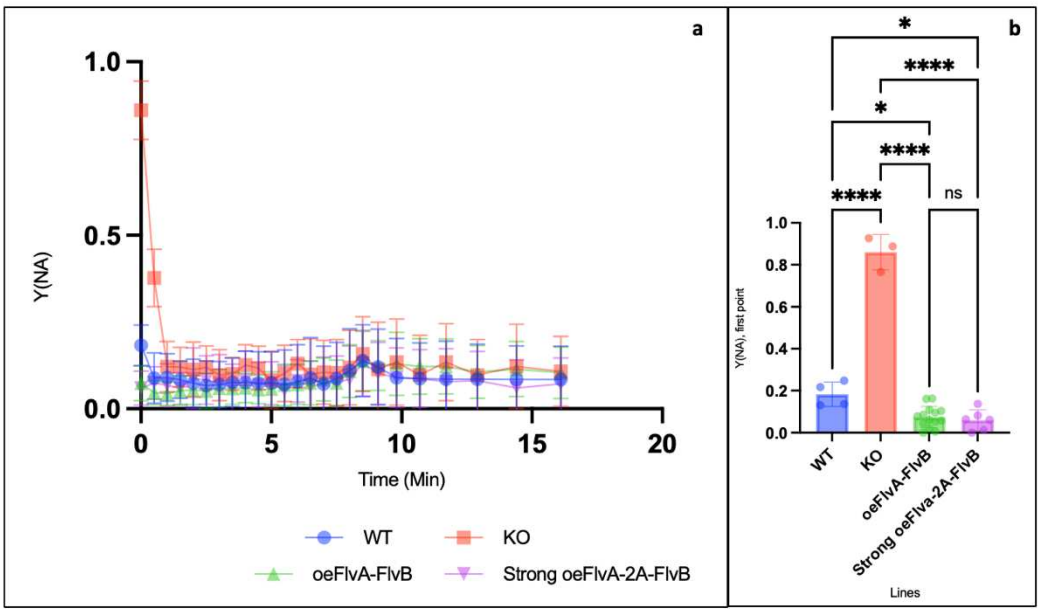

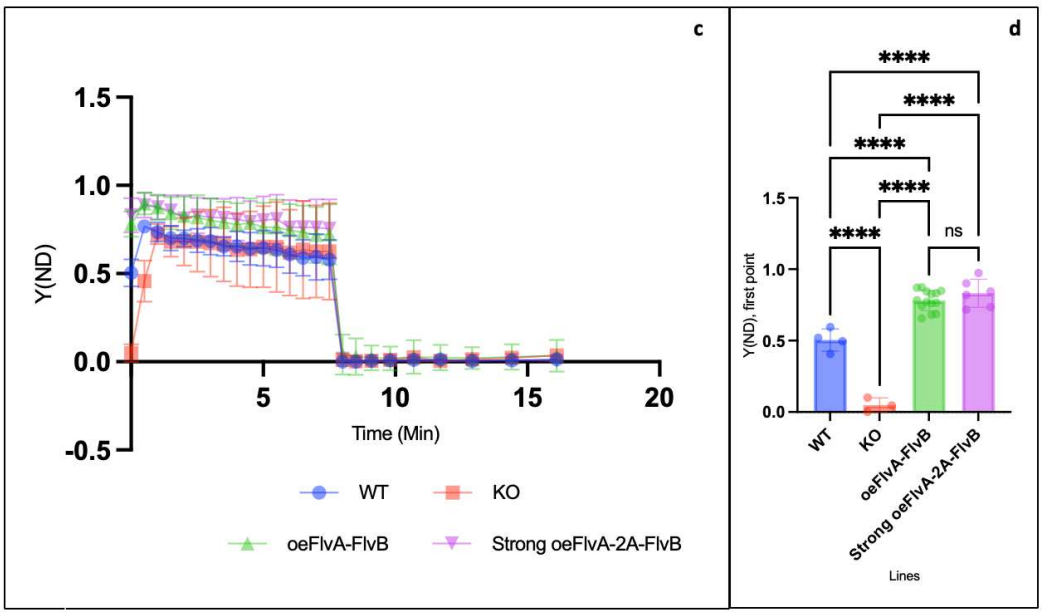

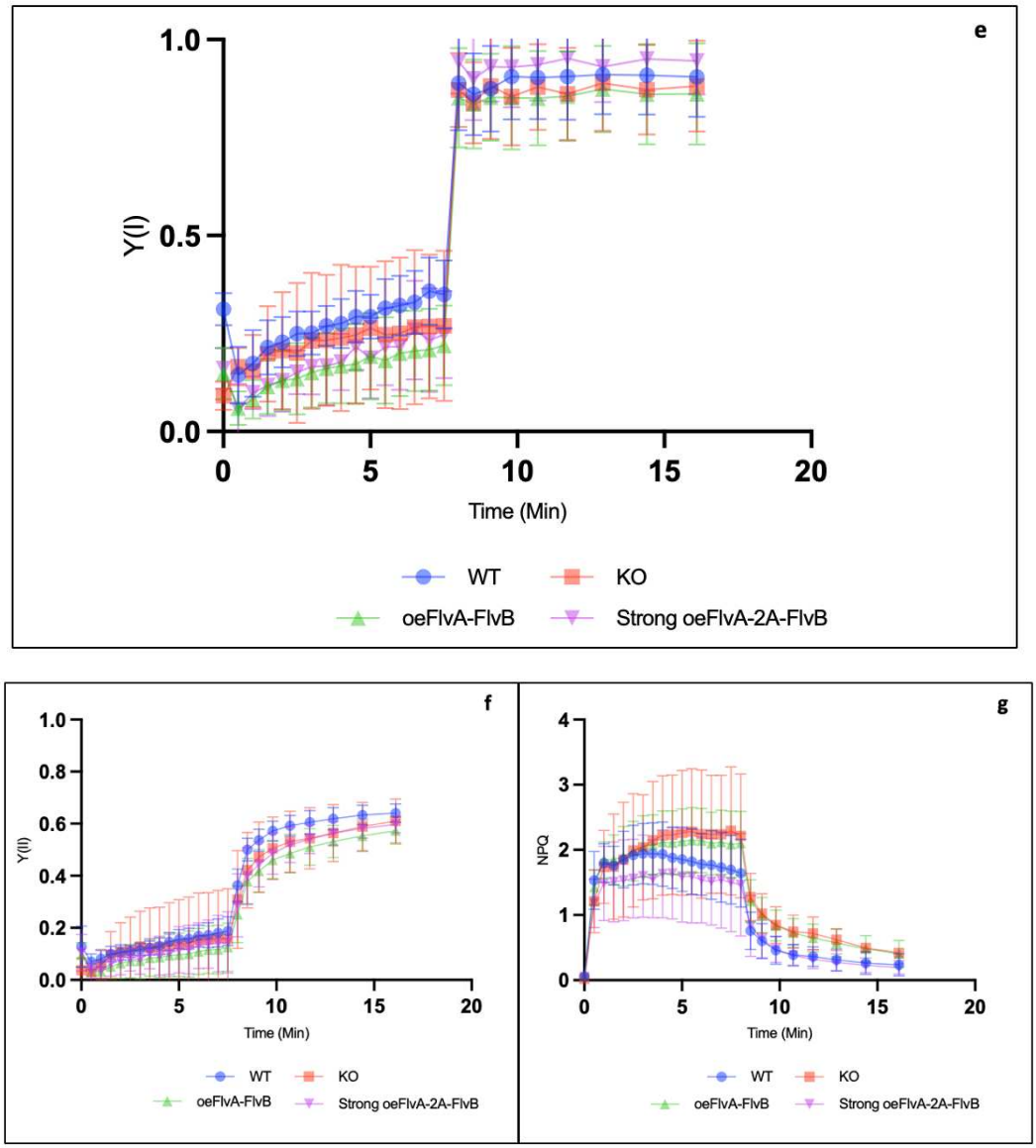

***Figure 3.5.1**: DUAL-PAM analysis performed on WT line (blue), KO line (red), oeFlvA-FlvB lines (green) and Strong oeFlvA-2A-FlvB lines (purple). The "Induction&Recovery" protocol has been applied (8 minutes of actinic light (AL), with a SP every 30 seconds, followed by 8 minutes of dark, with a SP at incremental intervals). The intensity of the AL was set at 500µmol photons $m^{-1}s^{-1}$. **a.** Y(NA) kinetics are reported for all the lines of interest. A focus is put on the first point of the kinetic of Y(NA). **b.** Histogram of the first point of Y(NA) for WT, KO, oeFlvA-FlvB lines (#8, #26, #30, #46 and #54) and Strong oeFlvA-2A-FlvB lines. The statistical analysis reveals a non-significative difference of oeFlvA-2A-FlvB lines compared with the WT and the oeFlvA-FlvB lines (one-way ANOVA, P>0.05). On the contrary, the negative control (KO) results significative difference compared with the WT, the oeFlvA-FlvB lines and the oeFlvA-2A-FlvB lines (one-way ANOVA, P<0.0001). **c.** Y(ND) kinetics are reported for all the lines. No significative differences have been detected (one-way ANOVA, P>0.05) **d.** A focus is put on the first point of the kinetic of Y(ND), which appear significative difference between the oeFlvA-2A-FlvB lines and the two control lines, WT (one-way ANOVA, P<0.05) and KO (one-way ANOVA, P<0.0001). The relative histogram is reported. While no significative differences are detected between the oeFlvA-FlvB lines and the oeFlvA-2A-FlvB lines (one-way ANOVA, P>0.05), the WT and both the lines are significative different (one-way ANOVA, P<0.01 and one-way ANOVA, P<0.05, respectively). **e.** Y(I) (one-way ANOVA, P>0,05). **f.** Y(II) (one-way ANOVA, P>0,05). **g.** NPQ (one-way ANOVA, P>0,05).*

3.5.2 MILD oeFlvA-2A-FlvB LINES

As delineated in the previous results, a comprehensive characterization of the mild oeFlvA-2A-FlvB lines was conducted utilizing the Induction and Recovery protocol. These lines were systematically compared not only with the control lines but also with the strong oeFlvA-2A-FlvB lines.

In **Figure 3.5.2**, both the kinetic profile and the initial point of the Y(NA) parameter are presented. While the kinetic profile (**Figure 3.5.2a**) does not reveal noticeable differences between the analyzed lines, the histogram depicting the first point of Y(NA) (**Figure 3.5.2b**) provides more insightful information. Notably, the WT line, along with both strong and mild oeFlvA-2A-FlvB lines, exhibited lower levels of Y(NA) at the initial point compared to the knockout (KO). Statistical analysis revealed a significant difference between the negative control (KO) and the treated lines. Contrarily, non-significant differences were detected between the WT and both strong and mild oeFlvA-2A-FlvB lines.

Figure 3.5.2 also presents data related to the Y(ND) parameter. While the kinetic profile of Y(ND) (**Figure 3.5.2c**) did not exhibit significant differences, the initial point of Y(ND) revealed significative distinctions at the first second of the analysis. The histogram in **Figure 3.5.2d** underlines the difference between the *flva/flvb* KO, characterized by values close to 0, and the other lines, displaying higher values (around 1). Furthermore, no significant differences were observed between the positive control (WT) and both strong and mild oeFlvA-2A-FlvB lines. Interestingly, the mild oeFlvA-2A-FlvB lines show a slightly lower Y(ND) initial point compared to the strong oeFlvA-2A-FlvB lines, exhibiting a significant difference.

Additionally, Y(I), Y(II), and NPQ were subjected to analysis. The relative kinetic profiles are presented in **Figure 3.5.2e, f, g**, once again, no significant differences were detected through the statistical analysis.

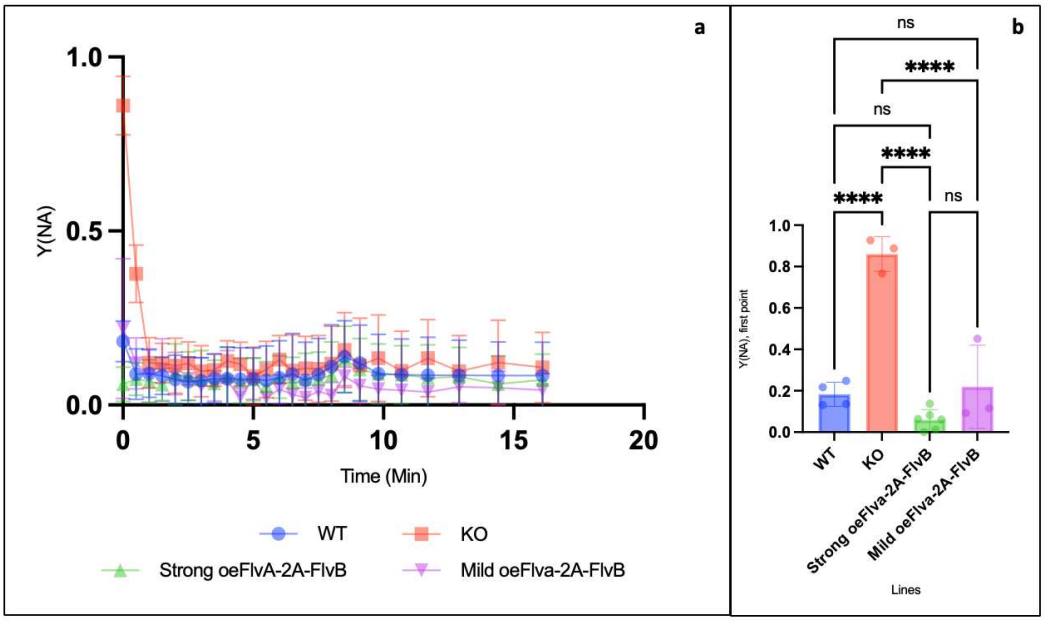
a
1.0
0.5
0.0
Y(NA)
0
5
10
15
20
Time (Min)
WT
KO
Strong oeFlvA-2A-FlvB
Mild oeFlva-2A-FlvB
b
ns
****
ns
****
****
ns
1.0
0.8
0.6
0.4
0.2
0.0
Y(NA), first point
WT
KO
Strong oeFlva-2A-FlvB
Mild oeFlva-2A-FlvB
Lines

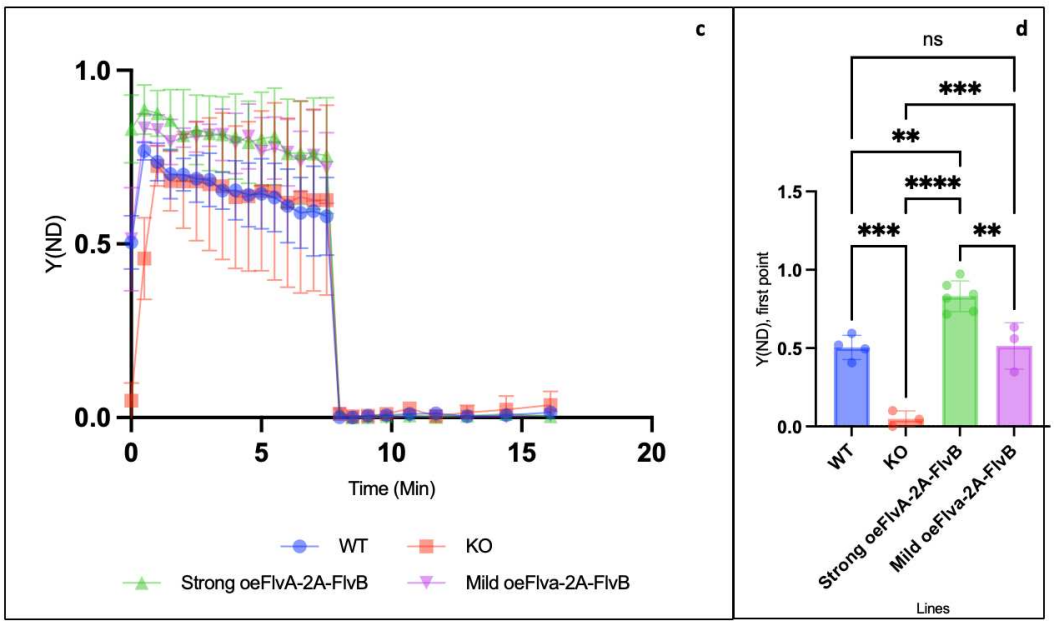
c
1.0
0.5
0.0
Y(ND)
0
5
10
15
20
Time (Min)
WT
KO
Strong oeFlvA-2A-FlvB
Mild oeFlva-2A-FlvB
d
ns
***
**
****
***
**
1.5
1.0
0.5
0.0
Y(ND), first point
WT
KO
Strong oeFlvA-2A-FlvB
Mild oeFlva-2A-FlvB
Lines

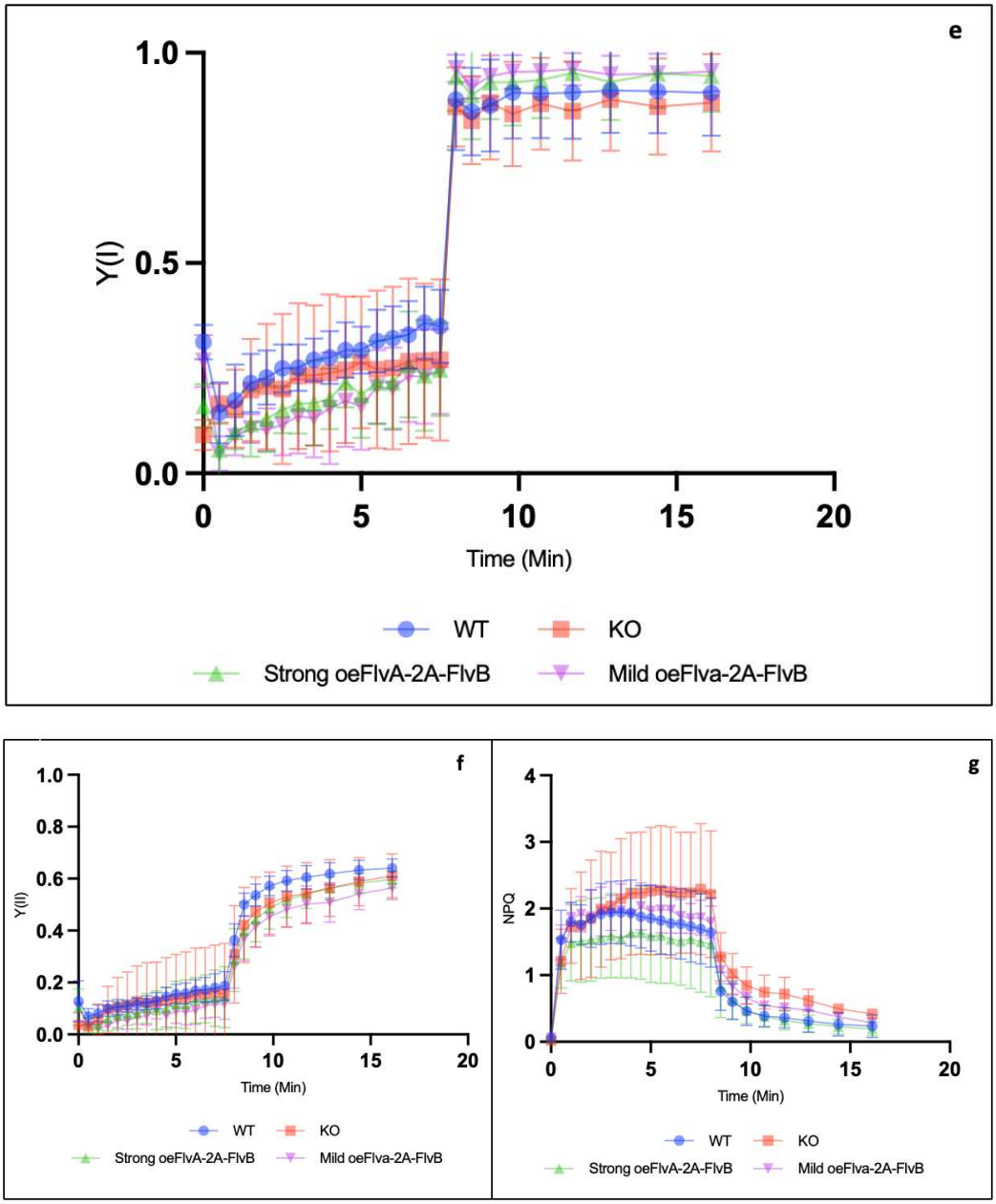

Figure 3.5.2: *DUAL-PAM analysis performed on WT line (blue), KO line (red), Strong oeFlvA-2A-FlvB (green), Mild oeFlvA-2A-FlvB lines (purple). The "Induction&Recovery" protocol has been applied (8 minutes of actinic light (AL), with a SP every 30 seconds, followed by 8 minutes of dark, with a SP at incremental intervals). The intensity of the AL was set at 500µmol photons $m^{-1}s^{-1}$.* ***a.*** *Y(NA) kinetics are reported for all the lines of interest. A focus is put on the first point of the kinetic of Y(NA).* ***b.*** *Histogram of the first point of Y(NA) all the lines. The statistical analysis reveals a significative difference between the KO and the WT and both strong and mild oeFlvA-2A-FlvB lines (one-way ANOVA, P<0.0001). No differences have been detected between the WT and both the strong and mild oeFlvA-2A-FlvB lines (one-way ANOVA, P>0.05).* ***c.*** *Y(ND) kinetics are reported for all the lines. The KO line results significative different from the WT and both strong and mild oeFlvA-2A-FlvB lines (one-way ANOVA, P<0.0001). A significative difference has been detected also between the WT and the strong oeFlvA-2A-FlvB lines, and between the strong and mild oeFlvA-2A-FlvB lines (one-way ANOVA P<0.001). No significative differences have been observed between the WT and the mild oeFlvA-2A-FlvB lines (one-way ANOVA, P>0.05).*

3.6 Flavodiiron proteins protect the photosystem I from photodamage under fluctuating light

In the data analysis, either the kinetics of Pm' and the Pm values, are reported, whereas Pm and Pm' represent the P700 signals recorded just before (P) then briefly after onset of a saturating pulse (Storti et al. 2019). In the first case it is possible to appreciate the variation of Pm' all along the measurement, while the second gives information about the fraction of PSI still able to perform charge separation. To obtain this data, the following formula has been used:

$$\%Pm = \frac{Pm_3 \times 100}{Pm_1}$$

where, Pm_3 indicated the last Pm recorded while Pm_1 represent the first one.

Previous studies reveal that flavodiiron proteins protect the photosystem I from the overreduction of the electron transport chain during stress light conditions (Alboresi, Storti, e Morosinotto 2019).
Thus oeFlvA-FlvB, oeFlvB and oeFlvA-2A-FlvB lines have been exposed to a "Fluctuating Light Protocol" (see material and method section). More precisely, the maximal level of oxidized PSI (Pm) has been analyzed, both at the beginning and at the end of the experiment.
In detail, the 1h fluctuating light protocol is characterized by the reinteraction of 1 minute of high light (800µmol photons $m^{-1}s^{-1}$), followed by 4 minutes of darkness.

3.6.1 FLUCTUATING LIGHT PROTOCOL ON oeFlvA-FlvB LINES

In the **Figure 3.6.1**, graphs resulting from the data processing are reported.
The kinetic of the Pm' parameter show a significative difference between the KO and the WT, but also between the KO and the oeFlvA-FlvB lines (**Figure 3.6.1a**). It is interesting to appreciate that *flva/flvb* KO Pm' immediately dropped to 0 for the whole duration of the analysis, while WT and oeFlvA-FlvB lines values are constantly around 0,350.

The PSI fraction (that has not been damaged after the fluctuating light exposure is reported in **Figure 3.6.1b**). A significative difference has been observed between the WT (81%) and the KO (41%) while, no significative difference has been detected between the WT and all oeFlvA-FlvB lines, indicating a completely rescue of the phenotype in the oeFlvA-FlvB lines.

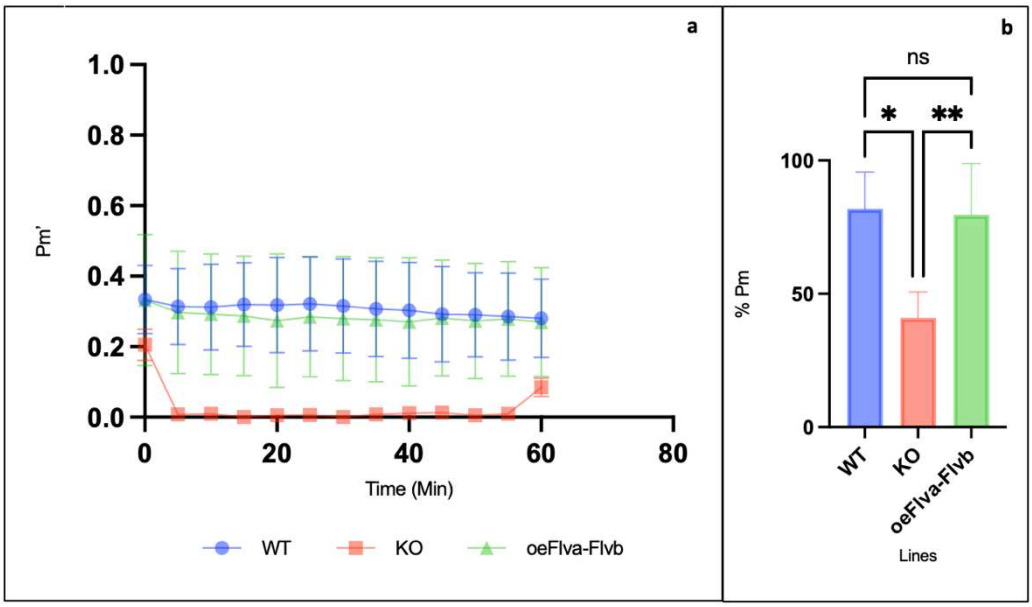

***Figure 3.6.1**: DUAL-PAM analysis performed on WT line (blue), KO line (red) and oeFlvA-FlvB lines (green). The latter results from four different lines (#8, #30, #46 and #54) for which four replicas were performed and mediated. The Fluctuating Light protocol has been applied: 1 minute of high light (800µmol photons $m^{-1}s^{-1}$), followed by 4 minutes of dark. The latter is the repeated for the whole duration of the analysis, 1h. **a.** Pm kinetic for the WT, the KO and the oeFlvA-FlvB lines. Statistical analysis results significative between the WT and the KO one-way ANOVA, P<0.0001), and between the KO and the oeFlvA-FlvB lines (one-way ANOVA, P<0.001). On the contrary, any significative difference has been observed between the WT and the oeFlvA-FlvB lines. **b.** Histogram of the percentage of PSI that remain undamaged after the analysis. As observed in the kinetic, WT and oeFlvA-FlvB lines result significative different compared to the KO. Any significative difference has been observed between the WT and the oeFlvA-FlvB lines (one-way ANOVA, P>0.05).*

3.6.2 FLUCTUATING LIGHT PROTOCOL ON oeFlvB LINES

In oeFLVB lines (#7, #34), just FlvB is overexpressed. To better understand if FlvB is able to be functional active also in the absence of FlvA protein under fluctuating light, the Fluctuating Light protocol has been applied. As it has been done also in the previous paragraph, both the Pm' kinetic and the histogram of the Pm percentage are reported (**Figure 3.6.2**). In the first case (**Figure 3.6.2a**), it is possible to observe that *flva/flvb* KO and oeFLVB lines are characterized by a

kinetic that remain close to 0. A significative difference has been detected between both *flva/flvb* KO and oeFLVB lines compared to the WT. This result is further confirmed by a decrease in %Pm reported in the histogram in **Figure 3.6.2b**: while the fraction of not damaged PSI in WT resulted 82%, for *flva/flvb* KO and oeFlvB lines were respectively 41% and 59%.

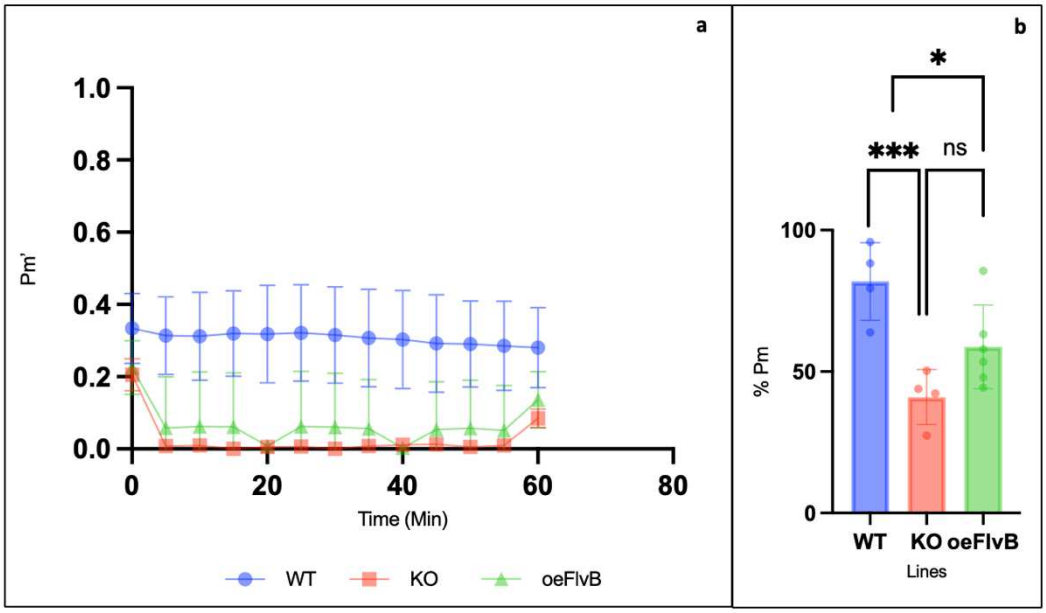

***Figure 3.6.2**: DUAL-PAM analysis performed on WT line (blue), KO line (red) and oeFlvB lines (green). The Fluctuating Light protocol has been applied: 1 minute of high light (800µmol photons $m^{-1}s^{-1}$), followed by 4 minutes of dark. The latter is the repeated for the whole duration of the analysis, 1h. **a.** Pm' kinetic for the WT, the KO and the oeFlvB lines. Statistical analysis results significative between the WT and the KO (one-way ANOVA, P<0.0001), and between the WT and the oeFlvB lines (one-way ANOVA, P<0.001). On the contrary, any significative difference has been observed between the KO and the oeFlvB lines. **b.** Histogram of the percentage of PSI still able to perform a charge separation at the end of the analysis. A significative difference has been detected between the WT and the KO (t test, P<0.0001), between the Wt and the oeFlvB (t test, P<0.0001), but no significative difference has been observed between the KO and the oeFlvB lines (t test, P>0.05).*

3.6.3 FLUCTUATING LIGHT PROTOCOL ON STRONG oeFlvA-2A-FlvB LINES

To further investigate on the effect of the presence of peptide 2A in strong oeFlvA-2A-FlvB lines, the Fluctuating light protocol has been applied in order to compare strong oeFlvA-2A-FlvB lines with oeFlvA-FlvB lines. In **Figure 3.6.3**, relative results are shown. The kinetic of Pm' parameter (**Figure 3.6.3a**) shows the fluctuation of Pm' during the protocol. In detail, the *flva/flvb* KO line remains

close to 0 for the whole duration of the experiment, while the WT, together with the oeFlvA-FlvB lines and the strong oeFlvA-2A-FlvB lines, exhibit level of Pm' between 0.2 and 0.35. Regarding the KO line it is possible to observe that the Pm value recorded at the beginning and at the end of the experiment assume higher values respect to the Pm' recorded during the protocol.

In **Figure 3.6.3b** the relative values of percentage of PSI able to perform a photochemical event after the end of the protocol are reported. In particular, it is possible to appreciate that no significative differences have emerged between the WT and the oeFlvA-FlvB lines (81%), and between the WT and the strong oeFlvA-2A-FlvB lines (96%). On the other hand, the just citated lines, show a significative difference with the KO (41%).

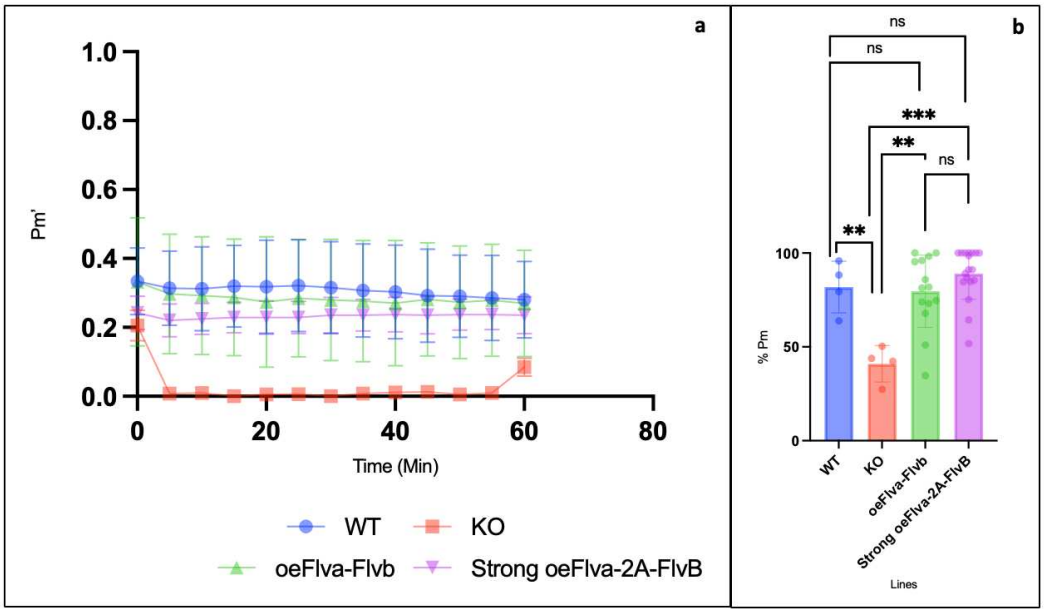

***Figure 3.6.3**: DUAL-PAM analysis performed on WT line (blue), KO line (red), oeFlvA-FlvB lines (green) and strong oeFlvA-2A-FlvB lines (purple). The Fluctuating Light protocol has been applied: 1 minute of high light (800µmol photons $m^{-1}s^{-1}$), followed by 4 minutes of dark. The latter is the repeated for the whole duration of the analysis, 1h. **a.** Pm' kinetic for all the lines. The KO line result significative different between the other lines (t test, P<0.0001) **b.** Histogram of the percentage of PSI still able to perform a charge separation at the end of the analysis. A significative difference has been detected between the WT and the KO (t test, P<0.001), between the KO and the oeFlvA-FlvB (t test, P<0.001) and also between the KO and the strong oeFlvA-2A-FlvB lines (t test, P<0.0001). No significative differences have been spotted between the WT and the oeFlvA-FlvB/strong oeFlvA-2A-FlvB lines, and between the mutants themselves (t test, P>0.05).*

3.6.4 FLUCTUATING LIGHT PROTOCOL ON MILD oeFlvA-2A-FlvB LINES

In order to understand the effect of the peptide 2A under fluctuating light in mild oeFlvA-2A-FlvB lines, DUAL-PAM instrument has been used together with the Fluorescence protocol. Such as for the last results, the kinetic of the Pm' has been reported in **Figure 3.6.4a**. The WT trace assume higher values respect to the other lines, with a Pm' around 0,3. Both the strong oeFlvA-2A-FlvB lines and the mild oeFlvA-2A-FlvB lines stay above the positive control. Differently, the KO trace is constantly close to 0, resulting significative different compared to the other tested lines.

Regarding the histogram in **Figure 3.6.4b**, no significative difference has been detected between the mild oeFlvA-2A-FlvB lines and the strong oeFlvA-2A-FlvB lines. Also, the WT is not different from the just citated lines. On the contrary, the KO (41%) results significative different compared to the WT (81%), the strong oeFlvA-2A-FlvB lines (96%) and the mild oeFlvA-2A-FlvB lines (100%).

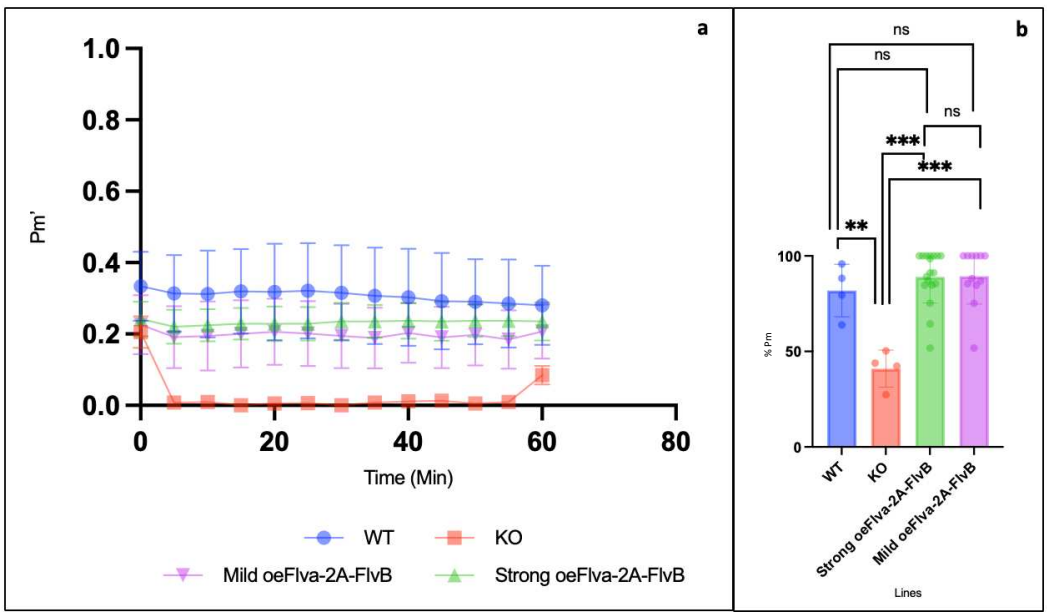

***Figure 3.6.4**: DUAL-PAM analysis performed on WT line (blue), KO line (red), strong oeFlvA-2A-FlvB lines (green) and mild oeFlvA-2A-FlvB lines (purple). The Fluctuating Light protocol has been applied: 1 minute of high light (800µmol photons $m^{-1}s^{-1}$), followed by 4 minutes of dark. The latter is the repeated for the whole duration of the analysis, 1h. **a.** Pm' kinetic for all the lines. The KO line result significative different between the other lines (t test, P<0.0001) **b.** Histogram of the percentage of PSI still able to perform a charge separation at the end of the analysis. A significative difference has been detected between the KO and all the lines tested. On the contrary, no significative differences have been observed between the WT and both the strong and mild oeFlvA-2A-FlvB lines (t test, P>0.05).*

6 Discussion

In plant systems, the linear electron transport (LEF), proceeding from water through photosystem II (PSII) and photosystem I (PSI) to reduce NADP+, is supplemented by different alternative electron transfer pathways. These alternative pathways play a fundamental role in plants responding to dynamic environmental fluctuations, such as stress conditions or sudden alterations in light intensity. One universally conserved pathway is the flavodiiron protein (FDP)-mediated alternative electron transport from PSI to molecular oxygen (O_2). This pathway is operative across a broad spectrum of photosynthetic organisms, ranging from cyanobacteria to gymnosperms (Ilík et al. 2017).
In the following discussion, FlvA-FlvB lines and oeFlvA-2A-FlvB lines have been submitted to a series of experiments, in order to achieve the three main goals of these research.

6.1 Fluorescence protocol and molecular analysis to screen *P. patens* mutating lines

In the first part of the performed experiments, *P. patens* strains stably mutated for FLVA and FLVB genes (under a strong promoter, $P35_s$) have been used. With the purpose to select successfully transformed lines that survived to the antibiotic selection, the “Fluorescence Protocol” has been applied at the PAM-imaging instrument. As it has been described both in the introduction and in materials and methods, FLVs act downstream the PSI (Alboresi et al. 2019). Thus, in the dark-to-light transition, their absence leads to a decrease in the electron transport, with a consequent increase in term of fluorescence. Starting from the characterization of the two control lines, it has been possible to determinate the level of fluorescence in presence or absence of FLVs, respectively. As expected, the WT shows lower levels of fluorescence compared to the KO, due to FLVs ability to dissipate the energy in excess on the acceptor side of PSI. The level of fluorescence of the WT line (0.5) has been then used arbitrary to set a threshold to discriminate clones that functionally express FLVs from the others. In (**Figure 3.1b**), a focus on the first seconds of the analysis shows if the tested lines resulted more similar to the WT or to the KO. This information helped us to understand the probability of expression of the FLVs in these lines. In fact, lines

with high levels of fluorescence indicate a low level of probability to express functional FLVs, due to their incapacity to protect the PSI from photodamage. For all the tested lines, results are reported in **Figure 3.1c**. After the actinic light is switched on, mutant lines divided into two groups: one more similar to the WT and one characterized by values closer to the KO. Based on what has been just said, the latter seems has a low probability to express FLVs proteins, also if the lines included in this group survived at the antibiotic selection.
From the moment it is not possible to know the precise level of expression of FLVs just applying the fluorescence protocol, molecular analysis has been performed (**Figure 3.2**). In point of fact, western blots helped us to classify the tested lines into different groups, based on the level of accumulation of FLVs. It is noteworthy to note that all the lines that show level of fluorescence lower respect to the positive control (<0.5) are the same lines that show an over expression of FLVs, oeFlvB-FlvA lines, suggesting that a higher expression of FLVs is correlated with lower level of fluorescence. On the other hand, those lines that behave more like the KO, express low or null levels of FLVs. Among these last, also oeFlvB lines are included, indicating a low efficiency in term of energy dissipation in lines that over express just FlvB. The so called “WT-like” lines show a particular level of fluorescence. In fact, also if molecular analysis indicates similar level of FLVs expression when compared to the WT, the level of fluorescence is intermedia. Further analysis should be performed on these lines. Since FLVs are known to be functionally active as a heterodimer (Alboresi et al. 2019), a linear regression of the data coming from quantification of the FlvA and FlvB optical density of the immunoblot bands has been performed. The R^2 value is positive, but the low number of replicas didn’t allow to perform the statistical analysis.

6.2 The effect of the over expression of FLVs under high light and fluctuating light

Results obtained with the previous screening allowed to better understand the effect of the accumulation of FLVs. Many parameters can be obtained using the DUAL-PAM instrument. Among these, the Y(NA) is the one that, together with the Y(ND) parameter, can inform us about the state downstream and upstream of the PSI. As it has been reported in the results (**Figure 3.3**), the first point of

these two parameters informs about the effect of the over-expression of FLVs. Data coming from oeFlvA-FlvB lines confirm what it has been just said, showing a significative difference with the KO, but also with the WT, indicating a better efficiency in term of Y(NA) and Y(ND). About their relative kinetic, besides the first point, the high intensity of the AL didn't allow to see a significative difference between the over expressing lines and both the WT and the *flva/flvb* KO. The same phenome has been observed in the kinetics related to the Y(I), the NPQ and the Y(II), suggesting that the AL intensity (500µmol photons $m^{-1}s^{-1}$) was already high enough to reach the maximal values in these parameters. Unfortunately, any replica with lower light intensity has been performed.
Since it has been observed that FLVs act as a safety valve of electrons under fluctuating light (Alboresi et al. 2019), the "Fluctuating Light Protocol" has been applied on oeFlvA-FlvB lines to investigate on the level of Pm and on the kinetic relative to the Pm'.
As expected, results related to the KO showed an over reduction of the PSI, suggesting that lines that do not express FLVs were unable to perform photochemistry reactions under fluctuating light. On the contrary, looking at the WT and the oeFlvA-FlvB lines, it was possible to observe that both lines showed similar kinetics and higher values of Pm' compared to the KO, indicating a complete rescue of the phenotype by oeFlvA-FlvB lines.

6.3 The effect of the over expression of just FlvB under high light and fluctuating light

In order to understand if FlvB protein is able to protect the PSI from photodamage in absence of FlvA, oeFlvB lines were exploited. As mentioned in the last paragraph, the analyzed kinetics related to photosynthetic parameters coming from the DUAL-PAM didn't show any difference between the WT, the KO and the oeFlvB lines, due to the saturating intensity of the AL. Contrary, if we moved our attention on the first point of the kinetics, significative differences emerged. In detail, regarding the Y(NA) parameter, oeFlvB lines results significative different between both WT ad KO. oeFlvB lines values at the first point are even higher respect to the KO, thus it's probably that the over expression of just FlvB has a worst effect on the efficiency in term of Y(NA) compared to the *flva/flvb* KO line. The first point of Y(ND) parameter shows a

significative difference between the oeFlvB lines and the WT, but no significative difference has been detected between the oeFlvB lines and the KO. Thus, no rescue of the phenotype in term of Y(ND) has been observed. Finally, kinetics of the Y(I), the Y(II) and the NPQ, except at the first point. No statistical analysis has been conducted on these data (**Figure 3.4**).
Results obtained with the "Fluctuating Light Protocol" are reported in **Figure 3.6.2**. Due to the impossibility to work as a heterodimer, the over expression of just FlvB don't lead to a rescue of the phenotype. As it is possible to observe in the kinetic, the level of Pm' during the protocol is quite close to the one related to the *flva/flvb* KO. On the contrary, the WT demonstrate that the fraction of PSI able to perform photochemistry in presence of FLVs under fluctuating light is higher compared to the oeFlvB lines and the KO, confirming the activity of FLVs proteins under this light condition.
The analysis of the percentage of PSI able to perform a charge separation at the end of the experiment have been reported in a histogram. Any significative difference between the oeFlvB lines and the *flva/flvb* KO have been observed, confirming again that oeFlvB lines don't show a rescue of the phenotype under fluctuating light condition.

6.4 Physiological analysis of strong and mild oeFlvA-2A-FlvB lines: the effect of the 2A peptide

To understand whether or not the peptide 2A has an effect on the physiological functions, the strong and mild oeFlvA-2A-FlvB lines have been analyzed at the DUAL-PAM instrument. If the presence of the peptide 2A has no effect on the physiological parameters of strong oeFlvA-2A-FlvB lines, results coming from the Induction and Recovery protocol and from the Fluctuating Light protocol shouldn't be different from those of oeFlvA-FlvB lines.
Data analysis coming from the comparison between the strong oeFlvA-2A-FlvB lines and the oeFlvA-FlvB lines (**Figure 3.5.1**) didn't show significative difference, suggesting any significative effect of the peptide 2A at the level of the Y(NA). Also, the Y(ND) didn't reveal any difference between the two over expressing lines, indicating once again that the peptide 2A hasn't any significative effect on this physiological parameter. The comparison between the strong oeFlvA-2A-FlvB lines and the oeFlvA-FlvB lines with the flva/flvb KO underlie the relevance

of the expression of the FLVs under high light in P. patens. In fact, the absence of these proteins leads to a lower Y(NA) efficiency (higher value of Y(NA)) and lower efficiency in term of Y(ND) (higher value of Y(ND)), with a consequent negative impact on the physiological processes. Surprisingly, both FLVs over expressing lines results significative different from the WT, showing lower value Y(NA) and thus, a better efficiency in term of it. The same difference has been observed in the graphs regard the Y(ND), where the strong oeFlvA-2A-FlvB lines and the oeFlvA-FlvB lines show a better efficiency of the Y(ND).
The analysis of the kinetics of Y(I), Y(II) and NPQ should allowed us to effectively understand the effect of the peptide 2A on the overall physiological status. Unfortunately, the saturating level of the AL didn't permit to observe any difference between the tested lines.
Under fluctuating light condition the strong oeFlvA-2A-FlvB lines, the oeFlvA-FlvB lines and the WT didn't show any difference in the kinetics related to the Pm', suggesting a complete rescue of the phenotype (**Figure 3.6.3**). Thus, the fraction of PSI able to perform a charge separation in the strong oeFlvA-2A-FlvB lines is similar to the one in oeFlvA-FlvB lines and in the WT. It's important to notice that in absence of FlvA and FlvB, the level of PSI able to oxidize and perform a charge separation is close 0. The *flva/flvb* KO is in fact unable to perform charge separation under fluctuating light compared to the over expression lines and the WT.
The histogram related to the percentages of PSI able to be oxidized at the end of the fluctuating light protocol, show a significative difference between the KO and the WT, but also between the KO and both the strong oeFlvA-2A-FlvB lines and the oeFlvA-FlvB lines. Indeed, only the 41% of the PSI are able to be oxidize at the end of the experiment; diversly, the 81% and the 96% of the PSI are able to be oxidase in the oeFlvA-FlvB lines and in the strong oeFlvA-2A-FlvB lines respectively. Any significative difference has been detected between the two over expressing lines, suggesting a non-significative impact of the peptide 2A under fluctuating light.

While the strong oeFlvA-2A-FlvB lines express the FLVs proteins 10 times more respect to the WT, the mild oeFlvA-2A-FlvB lines express FLVs just 1 or 2 times more. When compared to the strong oeFlvA-2A-FlvB lines under high light (**Figure 3.5.2**), any significative difference emerged at the level of Y(NA) kinetic, but also at the level of the first point of Y(NA). It seemed that the over expression of FLVs in the strong oeFlvA-2A-FlvB lines do not lead to a better

efficiency compared to the mild oeFlvA-2A-FlvB lines. This can be due to the fact that FLVs proteins represent a PCEF pathway, thus the electrons are not recyclized into the electron transport chain, but they are exploited to produce water. Contrary to what we have just seen, at the level of the first point of the Y(ND), mild oeFlvA-2A-FlvB and strong oeFlvA-2A-FlvB lines are significative different. In fact, the efficiency in term of Y(ND) just after the light is switched on is better in the strong oeFlvA-2A-FlvB lines comparted to both the mild oeFlvA-2A-FlvB lines and the WT.

If we compared the WT with the mild oeFlvA-2A-FlvB lines, any difference emerges, suggesting similar phenotype.

The analysis of the Y(I), Y(II) and NPQ kinetics didn't show any significative difference. Further analysis with lower intensity of the AL should be perform.

Under fluctuating light (**Figure3.6.4**) no significative differences emerged and the overall kinetics of the mild oeFlvA-2A-FlvB and strong oeFlvA-2A-FlvB lines Pm' are similar to the WT, indicating a complete rescue of the phenotype. As expected, the KO Pm' results significative different from the other lines. Looking at the percentage of PSI able to be oxidized at the end of the 1h fluctuating protocol, it is possible to observe a significative difference between the KO and the FLVs expressing lines. On the contrary, no differences have been observed between the WT and both the mild oeFlvA-2A-FlvB and strong oeFlvA-2A-FlvB lines. Once again, strong oeFlvA-2A-FlvB lines result to not be advantaged respect to those lines that express 8 or 9 time less FLVs proteins.

Bibliography

Alboresi, Alessandro, Mattia Storti, Laura Cendron, e Tomas Morosinotto. 2019. «Role and Regulation of Class-C Flavodiiron Proteins in Photosynthetic Organisms». *Biochemical Journal* 476 (17): 2487–98. https://doi.org/10.1042/BCJ20180648.

Alboresi, Alessandro, Mattia Storti, e Tomas Morosinotto. 2019. «Balancing Protection and Efficiency in the Regulation of Photosynthetic Electron Transport across Plant Evolution». *New Phytologist* 221 (1): 105–9. https://doi.org/10.1111/nph.15372.

Fischer, Woodward W., James Hemp, e Jena E. Johnson. 2016. «Evolution of Oxygenic Photosynthesis». *Annual Review of Earth and Planetary Sciences* 44 (1): 647–83. https://doi.org/10.1146/annurev-earth-060313-054810.

Folgosa, Filipe, Maria C Martins, e Miguel Teixeira. 2018. «Diversity and Complexity of Flavodiiron NO/O2 Reductases». *FEMS Microbiology Letters* 365 (3). https://doi.org/10.1093/femsle/fnx267.

Gao, Jinlan, Hao Wang, Qipeng Yuan, e Yue Feng. 2018. «Structure and Function of the Photosystem Supercomplexes». *Frontiers in Plant Science* 9 (marzo): 357. https://doi.org/10.3389/fpls.2018.00357.

Gurrieri, Libero, Francesca Sparla, Mirko Zaffagnini, e Paolo Trost. 2023. «Dark Complexes of the Calvin-Benson Cycle in a Physiological Perspective». *Seminars in Cell & Developmental Biology*, marzo, S1084952123000496. https://doi.org/10.1016/j.semcdb.2023.03.002.

Ilík, Petr, Andrej Pavlovič, Roman Kouřil, Alessandro Alboresi, Tomas Morosinotto, Yagut Allahverdiyeva, Eva-Mari Aro, Hiroshi Yamamoto, e Toshiharu Shikanai. 2017. «Alternative Electron Transport Mediated by Flavodiiron Proteins Is Operational in Organisms from Cyanobacteria up to Gymnosperms». *New Phytologist* 214 (3): 967–72. https://doi.org/10.1111/nph.14536.

Klughammer, Christof, e Ulrich Schreiber. 2008. «Saturation Pulse Method for Assessment of Energy Conversion in PS I».

Michelet, Laure, Mirko Zaffagnini, Samuel Morisse, Francesca Sparla, María Esther Pérez-Pérez, Francesco Francia, Antoine Danon, et al. 2013. «Redox Regulation of the Calvin–Benson Cycle: Something Old, Something New». *Frontiers in Plant Science* 4. https://doi.org/10.3389/fpls.2013.00470.

Murchie, E.H., e T. Lawson. 2013. «Chlorophyll Fluorescence Analysis: A Guide to Good Practice and Understanding Some New Applications». *Journal of Experimental Botany* 64 (13): 3983–98. https://doi.org/10.1093/jxb/ert208.

Nelson, Nathan, e Adam Ben-Shem. 2004. «The complex architecture of oxygenic photosynthesis». *Nature Reviews Molecular Cell Biology* 5 (12): 971–82. https://doi.org/10.1038/nrm1525.

Peterhansel, Christoph, Ina Horst, Markus Niessen, Christian Blume, Rashad Kebeish, Sophia Kürkcüoglu, e Fritz Kreuzaler. 2010. «Photorespiration». *The Arabidopsis Book* 8 (gennaio): e0130. https://doi.org/10.1199/tab.0130.

Rensing, Stefan A., Bernard Goffinet, Rabea Meyberg, Shu-Zon Wu, e Magdalena Bezanilla. 2020. «The Moss *Physcomitrium* (*Physcomitrella*) *Patens* : A Model Organism for Non-Seed Plants». *The Plant Cell* 32 (5): 1361–76. https://doi.org/10.1105/tpc.19.00828.

Rochaix, Jean-David. 2011. «Regulation of Photosynthetic Electron Transport». *Biochimica et Biophysica Acta (BBA) - Bioenergetics* 1807 (3): 375–83. https://doi.org/10.1016/j.bbabio.2010.11.010.

Schaefer, Didier G., e Jean-Pierre Zrÿd. 2001. «The Moss *Physcomitrella Patens* , Now and Then». *Plant Physiology* 127 (4): 1430–38. https://doi.org/10.1104/pp.010786.

Storti, Mattia, Alessandro Alboresi, Caterina Gerotto, Eva-Mari Aro, Giovanni Finazzi, e Tomas Morosinotto. 2019. «Role of Cyclic and Pseudo-cyclic Electron Transport in Response to Dynamic Light Changes in *PHYSCOMITRELLA PATENS*». *Plant, Cell & Environment* 42 (5): 1590–1602. https://doi.org/10.1111/pce.13493.

Yamamoto, Hiroshi, Shunichi Takahashi, Murray R. Badger, e Toshiharu Shikanai. 2016. «Artificial Remodelling of Alternative Electron Flow by Flavodiiron Proteins in Arabidopsis». *Nature Plants* 2 (3): 16012. https://doi.org/10.1038/nplants.2016.12.